



## Consistency of global MODIS aerosol optical depths over ocean on Terra and Aqua CERES SSF data sets

Alexander Ignatov,<sup>1</sup> Patrick Minnis,<sup>2</sup> Walter F. Miller,<sup>2,3</sup> Bruce A. Wielicki,<sup>2</sup> and Lorraine Remer<sup>4</sup>

Received 4 September 2005; revised 27 February 2006; accepted 30 March 2006; published 19 July 2006.

[1] Aerosol retrievals from the Moderate Resolution Imaging Spectroradiometer (MODIS) onboard Terra and Aqua platforms are available from the Clouds and the Earth's Radiant Energy System (CERES) Single Scanner Footprint (SSF) data sets. Over ocean, two aerosol products are reported side by side. The primary M product is generated by subsetting and remapping the multispectral (from 0.47 to 2.1  $\mu\text{m}$ ) MOD04/MYD04 oceanic aerosol data onto CERES footprints. M\*D04 processing uses cloud screening and aerosol algorithms developed by the MODIS science team. The secondary AVHRR-like A product is generated in only two MODIS bands. The A processing uses the CERES cloud-screening algorithm and NOAA/NESDIS glint identification and single-channel aerosol retrieval algorithms. The M and A products have been documented elsewhere and preliminarily compared using 2 weeks of global Terra CERES SSF edition 1A data, in which the M product was based on MOD04 collection 3. In this study, the comparisons between the M and A aerosol optical depths (AOD) in MODIS band 1 (0.64  $\mu\text{m}$ ),  $\tau_{1M}$  and  $\tau_{1A}$ , are reexamined using 9 days of global CERES SSF Terra edition 2A and Aqua edition 1B data from 13 to 21 October 2002 and extended to include cross-platform comparisons. The M and A products on the new CERES SSF release are generated using the same aerosol algorithms as before but with different preprocessing and sampling procedures, thus lending themselves to a simple sensitivity check to nonaerosol factors. Both  $\tau_{1M}$  and  $\tau_{1A}$  generally compare well across platforms. However, the M product shows larger differences, which increase with ambient cloud amount and toward the solar side of the orbit. The cross-platform, cross-product, and cross-release comparisons conducted in this study confirm an earlier observation that the major area for improvement in the current aerosol processing lies in a more formalized and standardized sampling (most importantly, cloud screening), whereas optimization of the aerosol algorithm is deemed to be an important yet less critical element.

**Citation:** Ignatov, A., P. Minnis, W. F. Miller, B. A. Wielicki, and L. Remer (2006), Consistency of global MODIS aerosol optical depths over ocean on Terra and Aqua CERES SSF data sets, *J. Geophys. Res.*, *111*, D14202, doi:10.1029/2005JD006645.

### 1. Introduction

[2] To improve our understanding of the Earth's radiation budget, the Terra and Aqua satellites carry four Clouds and the Earth's Radiant Energy System (CERES) scanners to measure the radiant energy exchange on Earth [Wielicki *et al.*, 1996]. CERES flight models 1 and 2 (FM1-2) have been operating on Terra since its launch into a 1030 Local Time (LT) Sun synchronous orbit in December 1999. Aqua, launched into a 1330 LT orbit in May 2002, carries flight

models 3 and 4 (FM3-4). The CERES Science Team generates Single Scanner Footprint (SSF) climate data records by combining CERES radiances with cloud and aerosol retrievals from the Moderate Resolution Imaging Spectroradiometer (MODIS) also onboard Terra and Aqua [Geier *et al.*, 2003]. Means and standard deviations of the finer resolution imager pixel radiances are calculated separately from the clear and cloudy portions within every CERES field of view (FOV) and reported in (larger size) CERES footprints, along with cloud/aerosol retrievals from these radiances. The spatial resolution (equivalent diameter at nadir) is 0.25–1 km for MODIS and  $\sim$ 20 km for CERES.

[3] These SSFs constitute an extremely valuable product for addressing the relationships between radiation, clouds and aerosols, not only because the essential parameters are well-matched in time and space, but also because they are providing a relatively long and continuous time series of measurements taken at two different times of day. To ensure that these products can be used confidently for studies of

<sup>1</sup>Office of Research and Applications, National Environmental Satellite, Data, and Information Service, NOAA, Camp Springs, Maryland, USA.

<sup>2</sup>Atmospheric Sciences, NASA Langley Research Center, Hampton, Virginia, USA.

<sup>3</sup>Science Applications International Corporation, Hampton, Virginia, USA.

<sup>4</sup>NASA Goddard Space Flight Center, Greenbelt, Maryland, USA.

climate-scale processes and diurnal changes, it is necessary to characterize the consistency of the retrieved parameters over time, across platforms, between processing releases, and between different algorithms. The consistency of the broadband radiance data and the CERES cloud retrievals have been described elsewhere [e.g., *Szewczyk et al.*, 2005; *Minnis et al.* 2004]. *Ignatov et al.* [2005] performed a preliminary analysis of an early release of the aerosol products on the Terra SSFs, but since then new product releases and Aqua data have become available requiring a more in-depth characterization of the CERES aerosol products.

[4] Over ocean, two aerosol products are reported for each CERES footprint on the SSF, both derived from MODIS, yet using different sampling and aerosol algorithms [*Ignatov et al.*, 2005]. The primary M product is derived from the standard M\*D04 granules (termed MOD04 for Terra and MYD04 for Aqua), developed by the MODIS Science Team, whereas a simpler secondary AVHRR-like A product is produced by the CERES Science Team with a less sophisticated cloud clearing, more restrictive glint screening and a single-channel NESDIS aerosol algorithm. The A product serves as a backup for the M product. Also, it is helpful to place the 27+ year NOAA AVHRR, and the 7+ year Tropical Rainfall Measuring Mission (TRMM) Visible and Infra-Red Scanner (VIRS) heritage aerosol records in context of the more accurate M aerosols, and to quantify the MODIS multichannel improvements. The M and A products on the Terra and Aqua CERES SSF data sets were described in detail by *Ignatov et al.* [2005] and are only briefly summarized in section 2.

[5] This paper reexamines, in detail, the earlier results reported in *Ignatov et al.* [2005] for Terra edition 1A, with the latest and improved SSF releases for Terra edition 2A and Aqua edition 1B. The focus is on the cross-product, cross-platform, and cross-release consistency of M and A AOD retrievals in MODIS band 1,  $\tau_{1M}$  and  $\tau_{1A}$ . All changes between the two SSF releases were in the respective preprocessing (such as calibration or normalization of satellite radiances to solar flux) and sampling (i.e., selection of the aerosol pixels to be used in the aerosol inversions) procedures, and there was no change in either of the M or A aerosol algorithm (i.e., inversion of MODIS radiances to aerosol parameters). Nevertheless, both aerosol products show measurable sensitivity to such nonaerosol changes.

## 2. Two Aerosol Products Over Ocean on the CERES SSF Data Sets

[6] The primary M aerosol product is generated by subsetting and remapping the 10-km M\*D04 granules onto ~20-km (at nadir) CERES footprints. The M\*D04 processing uses sophisticated cloud screening and multispectral (6 bands from 0.55 to 2.1  $\mu\text{m}$ ) aerosol retrieval algorithms developed by the MODIS cloud and aerosol groups [*Ackerman et al.* 1998; *Tanré et al.*, 1997; *Martins et al.*, 2002; *Remer et al.*, 2005]. Fifteen of the 29 aerosol parameters reported in each M\*D04 granule over ocean are saved on the CERES SSF. Only one of them is analyzed in this study, the M aerosol optical depth (AOD),  $\tau_{1M}$ , reported at the central wavelength of MODIS band 1,  $\lambda_{1M} = 0.644 \mu\text{m}$ .

[7] The secondary A product uses a different glint and cloud screening and a simpler AVHRR-like third-generation

NESDIS aerosol algorithm [*Ignatov et al.*, 2005]. Two AODs,  $\tau_{1A}$  (0.630  $\mu\text{m}$ ) and  $\tau_{2A}$  (1.610  $\mu\text{m}$ ) are derived from MODIS bands 1 and 6 using two independent single-channel algorithms. (On Aqua,  $\tau_{2A}$  at 2.113  $\mu\text{m}$  is derived from band 7.) The respective look-up tables were calculated separately for Terra and Aqua, taking into account the exact spectral response functions of their MODIS sensors. Only  $\tau_{1A}$  is analyzed in this study reported at the wavelength  $\lambda_{1A} = 0.630 \mu\text{m}$ .

[8] The A aerosol algorithm is currently employed to analyze data from AVHRR/3 on the NOAA 16, 17, and 18 platforms, VIRS on TRMM, and MODIS on Terra and Aqua [*Ignatov et al.*, 2004b, 2005]. More recently, it was tested using data from the Spinning Enhanced Visible and Infrared Imager (SEVIRI) onboard Meteosat Second Generation (MSG, renamed to Meteosat 8 after launch in 2002), the first successful test of the A algorithm with geostationary data [*Brindley and Ignatov*, 2006]. Note that all A products, derived from different platforms and sensors, are consistently reported at standard wavelengths representative of the band centers for a generic AVHRR sensor, thus facilitating their cross-platform comparisons.

[9] In both products, Sun glint areas are excluded by only making retrievals outside the  $\gamma = 40^\circ$  cone glint angle. Additionally, all data from the solar side of the orbit are excluded in the A product for historical reasons. This restriction reduces the number of A samples compared to the M samples and is currently being reevaluated.

[10] The cross-platform comparisons include a 3-hour time difference between the midmorning Terra and early afternoon Aqua platforms. Figure 1 shows that since their launch, Terra and Aqua have typically been crossing the equator within 15 and 5 min of their nominal equatorial crossing times, respectively. However, local solar time of the aerosol observations may be shifted by an hour or two with respect to the equator crossing time due to the MODIS cross-track scan, the satellite orbital inclination, and product specifics (see example in Figure 2). According to *Kaufman et al.* [2000], AOD diurnal variations over open oceans are small, and should not affect results of cross-platform comparisons.

## 3. Data

[11] This study uses 9 days of global Terra CERES/FM1 (edition 2A) and Aqua CERES/FM4 (edition 1B) SSF M and A aerosol data from 13 to 21 October 2002. The CERES FM1 and FM4 data sets were chosen because both instruments operated in a cross-track mode during October 2002, thereby providing uniform coverage, whereas their “twins”, FM2 on Terra and FM3 on Aqua, operated in the rotating azimuth plane (RAP) mode. Aerosol products reported on the RAP SSFs on the same platforms are derived from the same MODIS instrument and therefore should be identical. However, in fact, the fields of view of the two CERES instruments on the same satellite can significantly differ in size even though they are nearly collocated when scanning in the two modes. Geographical coregistration of the aerosol products reported at the centers of CERES footprints is more accurate when the instrument is in a cross-track mode and the CERES FOVs are generally smaller [*Ignatov et al.*, 2005].

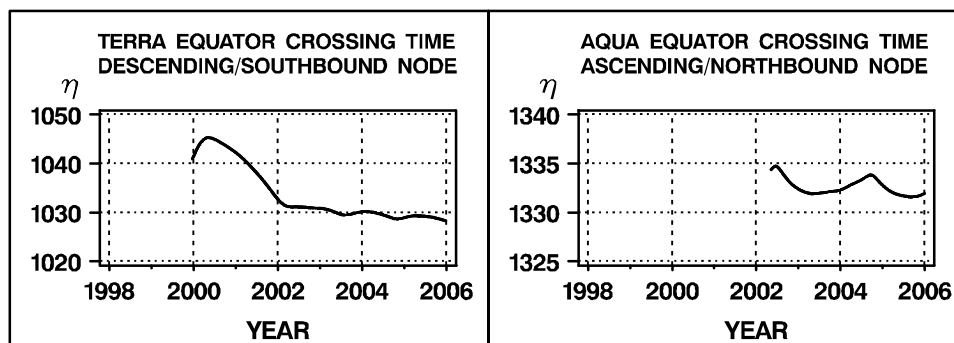


**Figure 1.** Local equator crossing time,  $\eta$ (h), for the Terra and Aqua platforms. Data are the two-line element from Celestrack (<http://www.celestrak.com>). Note that the nominal EXTs are 1030 for Terra and 0130 for Aqua. For details, see *Ignatov et al.* [2004a].

[12] To evaluate aerosol improvements in this new SSF release (Terra edition 2A and Aqua edition 1B), we employ data for the same 9-day period, but from the previous SSF release (Terra edition 1A and Aqua Beta1). The SSF Beta versions are not considered official by the CERES Science Team and not approved for public distribution. However, an exception to this rule was made here because no official Aqua SSF data are available based on the previous SSF processor, whereas the Aqua Beta1 processor was similar to that used for Terra edition 1A.

[13] The A SSF processing uses 1-km resolution MODIS L1b data as input and first subsamples them to save disk space and processing time. Every other scan line is used in both versions, while every other pixel was used in the earlier version and every fourth pixel is used in the later version. Then M aerosol properties are assigned to each subsampled 1-km MODIS L1b pixel from the 10-km M\*D04 L2 granule that contains that pixel, whereas the A “aerosol pixels” are identified by the A cloud and glint screening. One of the most important cloud tests in the A aerosol processing is the spatial uniformity test. It is applied to  $2 \times 2$  arrays of subsampled pixels and requires that the difference between the maximum and minimum reflectances in MODIS band 1 does not exceed 0.003 (0.3%). As a result, the new test is more conservative because the same threshold is now applied to pixels separated by  $4 \times 8$  km compared to the previous separation of  $4 \times 4$  km. An

additional adjacency test is then applied that requires that all pixels surrounding a candidate A pixel must be clear. The M\*D04 processing also employs a spatial uniformity test applied to  $3 \times 3$  arrays of 500-m MODIS reflectances in band 4 ( $0.555 \mu\text{m}$ ) with a requirement that the standard deviation is less than 0.0025 (0.25%) for the central pixel to be considered cloud-free [*Martins et al.*, 2002; *Remer et al.*, 2005]. In both the A and M processing, the spatial uniformity thresholds are assumed globally nonvariable and independent of view and illumination geometry.

[14] Next, the (subsampled) pixel-level M aerosol properties (from M\*D04) and the A screened radiances are convolved into the corresponding CERES footprint using the CERES point spread function, and the A aerosol properties are derived from the convolved radiances [*Geier et al.*, 2003]. To reduce processing time and data volume, certain CERES footprints are removed in the new SSF release. A given CERES footprint may overlap the adjacent footprint by up to 80%, especially for the near-nadir footprints. Thus thinning out highly overlapped CERES FOVs is expected to have a minimal impact on gridded products. The specifics of the sampling algorithm and its evolution can be found at [http://eosweb.larc.nasa.gov/GUIDE/dataset\\_documents/cer\\_ssf\\_trmm\\_pfm\\_edition1.html](http://eosweb.larc.nasa.gov/GUIDE/dataset_documents/cer_ssf_trmm_pfm_edition1.html).

[15] There are other changes in the M and A products, in addition to the SSF sampling changes. The M processing in the previous Terra edition 1A SSF release was based on an

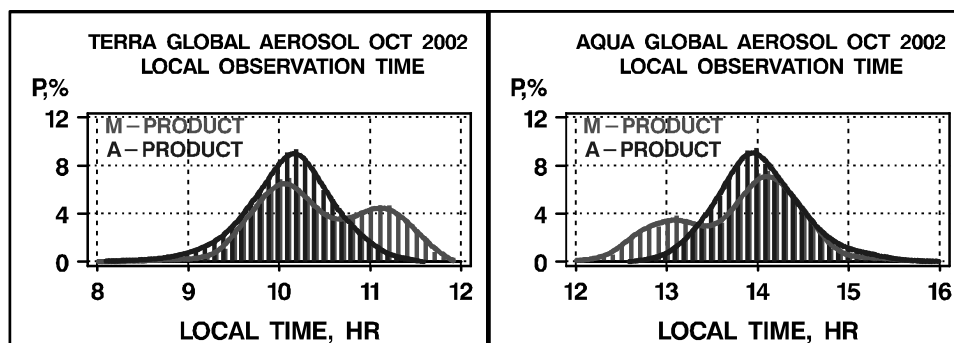


**Figure 2.** Frequency of local solar time in the M and A aerosol observations from Terra and Aqua platforms. Note that the solar side of orbit is excluded from the A product. As a result, its histogram is monomodal and shifted with respect to the equator crossing time toward lower Sun. The second peak in the M product comes from the solar side of the orbit.

**Table 1.** Global Mean Counts and Statistics of  $\tau_{1M}$  and  $\tau_{1A}$  and Auxiliary Parameters in CERES SSF Terra Edition 2A and Aqua Edition 1B data From 13 to 21 October 2002 Based on CERES FOVs and  $(1^\circ)^2$  Boxes<sup>a</sup>

	N	$\tau_{1M}$	LT, hours	$A_T$ , %	$\theta_v$ , deg	$\theta_s$ , deg	$\chi$ , deg	$\gamma$ , deg
Terra/M								
CERES FOVs	2,008,739	0.129	10.41	48.2	10.6	37.9	135.6	62.6
$(1^\circ)^2$ boxes	164,895	0.138	10.41	55.3	7.1	38.3	131.7	64.3
Aqua/M								
CERES FOVs	1,806,763	0.120	13.73	46.4	15.2	43.1	139.2	66.3
$(1^\circ)^2$ boxes	145,395	0.125	13.73	54.0	12.0	43.9	134.3	68.3
	N	$\tau_{1A}$	LT, hours	$A_T$ , %	$\theta_v$ , deg	$\theta_s$ , deg	$\chi$ , deg	$\gamma$ , deg
Terra/A								
CERES FOVs	932,810	0.133	10.17	32.5	32.6	37.3	149.8	64.2
$(1^\circ)^2$ boxes	81,426	0.135	10.08	41.3	36.7	39.5	146.7	69.2
Aqua/A								
CERES FOVs	951,832	0.130	13.90	30.6	30.2	42.0	152.5	68.2
$(1^\circ)^2$ boxes	80,573	0.132	13.99	39.9	34.7	44.1	150.1	74.0

<sup>a</sup>LT, local time;  $A_T$ , cloud amount, determined by the A processing;  $\theta_v$ , nadir view angle (defined as positive on antisolar and negative on solar side of orbit);  $\theta_s$ , solar zenith angle;  $\chi$ , scattering angle;  $\gamma$ , glint angle.

earlier MOD04 collection 3, whereas the Aqua Beta1 was based on MYD04 collection 4. The new SSF release consistently uses collection 4 products from both platforms (for a complete history of M\*D04 product evolution, see [http://modis-atmos.gsfc.nasa.gov/MOD04\\_L2/history.html](http://modis-atmos.gsfc.nasa.gov/MOD04_L2/history.html)). The A product in the new SSF release uses more accurate solar constants to convert radiances to reflectances (see section 5.3 for details). It is important to note however that there was no change in either M or A aerosol inversion algorithm from one SSF release to the other.

[16] Note that in the SSF data sets, the values of  $\tau_{1M}$  and  $\tau_{1A}$  are reported at slightly different wavelengths:  $\lambda_{1M} = 0.644$  and  $\lambda_{1A} = 0.630$   $\mu\text{m}$ , respectively. For the present comparisons,  $\tau_{1A}$  was first rescaled to the M wavelength of 0.644  $\mu\text{m}$  using particle properties assumed in the fixed A aerosol model as  $\tau_{1A}(0.644 \mu\text{m}) = 0.96377 \times \tau_{1A}(0.630 \mu\text{m})$  [Ignatov *et al.* 2005]. All  $\tau_1$  values in this report are given at the reference monochromatic wavelength of  $\lambda_{1M} = 0.644$   $\mu\text{m}$ .

[17] Besides  $\tau_{1M}$ , the M product reports six additional AODs in the MODIS aerosol bands 2–7 and the A product reports a second AOD,  $\tau_{2A}$  [Ignatov *et al.* 2005]. However, these additional AOD data are not analyzed here. The analyses are deliberately restricted to only one parameter in both products,  $\tau_1$  to keep this study in depth yet succinct. For instance, omitting  $\tau_{2A}$  values (which are retrieved from different MODIS bands on Terra (6) and Aqua (7)) eliminates the need to rescale them for cross-platform comparisons.

[18] The inoperative Aqua/MODIS band 6 is excluded not only from the A processing but from the MYD04 processing, too. Thanks to the flexibility of the M retrieval lookup tables, only a subset of bands can be used for retrievals [Tanré *et al.*, 1997]. Note however that MYD04 continues to report all seven AODs in MODIS bands 1–7, consistently with MOD04, the AOD in Aqua/MODIS band 6 being a mere interpolation to  $\lambda = 1.61$   $\mu\text{m}$  from the remaining 5 bands.) This treatment of band 6 on Aqua is fully analogous to the treatment of band 3 (0.47  $\mu\text{m}$ ) on both platforms. Recall that band 3 is not used in aerosol retrievals due to high and variable surface reflectance at 0.47  $\mu\text{m}$ . Nevertheless, AOD in this band is still derived by extrapolation of the aerosol model estimated from other MODIS

bands from 0.55 to 2.13  $\mu\text{m}$ , and reported on M\*D04.) In evaluating the results of cross-platform  $\tau_{1M}$  comparisons below, one should thus keep in mind that the M aerosol algorithm, although identical for Terra and Aqua, is nevertheless applied to a different set of MODIS bands (6 on Terra and only 5 on Aqua). Off-line tests to quantify the effect of excluding band 6 (or any other band) on the  $\tau_{1M}$  retrievals are possible using e.g., Terra MODIS data, where all six bands work nominally, but these analyses are beyond the scope of this study.

## 4. Summary Global Statistics

### 4.1. Statistics Derived From CERES Field of Views

[19] The odd data rows in Table 1 list the global CERES Field of views (FOV)-based statistics of  $\tau_{1M}$  and  $\tau_{1A}$  from Terra and Aqua, along with associated local time, cloud fraction, and retrieval geometry.

[20] Particular attention should be paid to the accurate definition of the cloud fraction parameter,  $A_T$ , which emerges as a key parameter in aerosol remote sensing (cf. analyses in section 6.1 below). The value listed in Table 1 and used throughout this paper has been determined by the CERES Team cloud mask processing [Minnis *et al.*, 2004]. Its two counterparts have been also derived by the MODIS Aerosol and Cloud Teams and available on the M\*D04 and M\*D06 granules. The M\*D04 cloud fraction was saved on the CERES SSF, but it is not used in this study.

[21] The global  $A_T$  statistics shown in Table 1 differ for the M and A products. This is because any CERES FOV with  $A_T = 100\%$  is not used to obtain the A aerosol product, but could have aerosol retrievals from the M product. Furthermore, vice versa, some CERES FOVs with valid A aerosols have no corresponding M values. Furthermore, all  $A_T$  statistics shown in Table 1 are conditional and therefore biased estimates since all CERES FOVs with no clear pixels (i.e.,  $A_T = 100\%$ ) are ignored in calculations.

[22] For a given CERES footprint, the A cloud fraction is defined as 100% minus percent clear fraction (defined as point spread function weighted fraction of MODIS pixels within a FOV that were determined as “clear” by the CERES Team cloud mask processing). We have chosen to

make this conversion, to emphasize the effect of ambient cloud on aerosol, but such defined cloud fraction may not be fully accurate as not all “nonclear” pixels are necessarily “cloudy”. Some of them may be simply missing e.g., due to poor quality data. Note also that aerosol fraction is also reported in each CERES FOV and it differs from the clear fraction as MODIS pixels within a FOV maybe clear but not used in aerosol retrievals (e.g., glint).

[23] In addition, as pointed out by *Brennan et al.* [2005], the definition of “cloud amount” depends upon application. For instance, the fraction of clear pixels used in aerosol retrievals tends to be smaller than one minus the fraction of cloudy pixels used in cloud retrievals, because either retrieval tends to classify questionable pixels in a counterpart category. Despite this tendency to be on a “safe side” in either product, which leaves a gray zone of unidentified pixels in between, *Brennan et al.* [2005] suggest that some fraction of the aerosol retrievals remains “cloud contaminated” as well as some fraction of cloud retrievals is still “aerosol contaminated.” The relative proportion of such “contaminated” pixels depends upon the specific cloud detection algorithm employed in the aerosol product.

[24] The following observations emerge from the CERES FOV statistics in Table 1.

[25] 1. First is cross-product sampling differences. The M sample size is twice that for the A product. This result is consistent with *Ignatov et al.* [2005]. Additional analyses (not shown) suggest that  $\sim 70\%$  of this difference is due to excluding the solar side of the orbit and viewing zenith angles  $\theta_v > 60^\circ$  in the A product, whereas the remaining  $\sim 30\%$  is due to a more conservative A cloud screening relative to the M screening. This result is consistent with the data in  $A_T$  column of Table 1 which shows that the average fraction of cloudy pixels is  $\sim 15\%$  larger in the M product than in the A product. It still remains to be seen which of the two cloud screenings perform better globally and regionally.

[26] 2. Second is cross-platform sampling differences. The Terra results yield 11% more CERES FOVs with valid M data than Aqua, and 2% fewer FOVs with valid A data. (In cross-platform sample size comparisons one should keep in mind that out of the total of 216 hours, 3 hours of Aqua edition 1B SSF data were missing (a 1.4% reduction) during this 9-day period because of CERES diagnostics.) The nature of the M cross-platform sampling differences is not immediately clear. Indeed, despite some orbital differences, Terra and Aqua cover almost identical geographical domains (as discussed in section 5.1). Their cross-platform cloud amount differences are also small and consistent, according to the CERES cloud mask:  $\Delta A_T = A_T(\text{Terra}) - A_T(\text{Aqua}) = 3.0\%$  and  $2.4\%$  in the M and A products, respectively.

[27] 3. Third is cross-product  $\tau_1$  differences. Generally,  $\tau_{1A}$  is larger than  $\tau_{1M}$ :  $\tau_{1A} - \tau_{1M} = 0.004$  for Terra and  $0.010$  for Aqua. Presumably, the algorithm-induced positive bias in the A product would be even greater, if the data selection were not constrained by the more conservative A cloud-screening process (see analyses in section 6.1). Data in Table 1 show the net effect of these two counterbalancing mechanisms.

[28] 4. Fourth is cross-platform  $\tau_1$  differences. In both products, the mean AODs are greater from Terra than from Aqua data:  $\Delta\tau_{1M} = 0.009$  and  $\Delta\tau_{1A} = 0.003$ . This bias could

be real indicating a systematic decrease in marine aerosol concentrations from morning to afternoon. Or, it may be due to differences in the illumination geometry that are not properly modeled by the respective retrieval algorithm. The mean value of  $\theta_s$  for Aqua, is  $5^\circ$  less than that for Terra, and the respective scattering and glint angles are  $3^\circ$ – $4^\circ$  larger than for Terra. The bias may also be due to residual cross-platform cloud screening differences (the Aqua screening is  $\sim 2$ – $3\%$  more conservative than Terra) or to a combination of viewing and screening differences.

#### 4.2. Aggregating CERES FOV Into Gridded $1^\circ$ Product

[29] For the analyses below, the global  $\tau_1$  retrievals and auxiliary parameters from 13 to 21 October 2002, reported for the CERES FOVs, were first remapped onto a regular grid and averaged, resulting in  $N = 164,895$  and  $N = 81,426$  ( $1^\circ$ )<sup>2</sup> boxes from Terra, and  $145,395$  and  $80,573$  from Aqua, with M and A aerosols, respectively. The  $1^\circ$  average cloud amount  $A_T$  parameter was calculated using only those CERES FOVs with valid aerosol retrieval in them, ignoring footprints with  $A_T = 100\%$ . Figure 3 (top) shows histograms of CERES FOV counts,  $N$ , used for calculating the average  $1^\circ$  statistics. The grid boxes are populated nonuniformly and the shapes of the histograms differ for the two products, due to differences in their sampling. Smaller values of  $N$  in a box are generally associated with more cloud or glint, or proximity to the coastline, scan edge, or Sun illumination limits. Figure 3 (bottom) plots the respective  $\tau_1(N)$  trends in the retrievals. The most prominent features in Figure 3 are as follows.

[30] 1. Both  $\tau_{1M}(N)$  and  $\tau_{1A}(N)$  increase toward low  $N$ . Greater uncertainties are expected in a product when approaching the boundaries of its valid domain. Figure 3 suggests that such difficulties are better mitigated in the A product, whose  $\tau_{1A}(N)$  trends are flatter and more consistent across platforms.

[31] 2. The minimum values of  $\tau_{1A}$  are informative about performance of the A algorithm and the calibration of band 1. For instance, close agreement between the values of  $\min(\tau_{1A})$  from Terra and Aqua indicates excellent calibration consistency between the two MODIS instruments. Simple estimates show that their bands 1 are consistent to within  $\sim 1$ – $2\%$  [*Ignatov*, 2002]. Another interesting feature of Figure 3 is the negative bias in  $\min(\tau_{1A})$  toward small values of  $N$ . The A algorithm does not truncate negative values of  $\tau_{1A}$  (which may result from e.g., radiometric errors, or occur when in situ Rayleigh optical depth is smaller than assumed in the retrievals). The latter happens when the water surface is elevated above the sea level. For example, the smallest  $\tau_{1A}$  are often associated with the least populated  $1^\circ$  boxes, typically found over high-altitude lakes [*Ignatov and Stowe*, 2002a]. In the M product, negative values of  $\tau_{1M}$  are currently truncated and therefore provide no information [*Ignatov et al.*, 2005].

[32] 3. The  $\tau_{1M}(N)$  trends in Terra and Aqua diverge for  $N < 20$  (where most M data are found), possibly indicating residual cross-platform cloud (see section 6.1) screening differences. Exclusion of band 6 from Aqua processing, or possible calibration differences in the MODIS bands used in aerosol retrievals, either directly (bands 1–2 and 4–7) or indirectly (e.g., thermal IR bands used in cloud clearing),

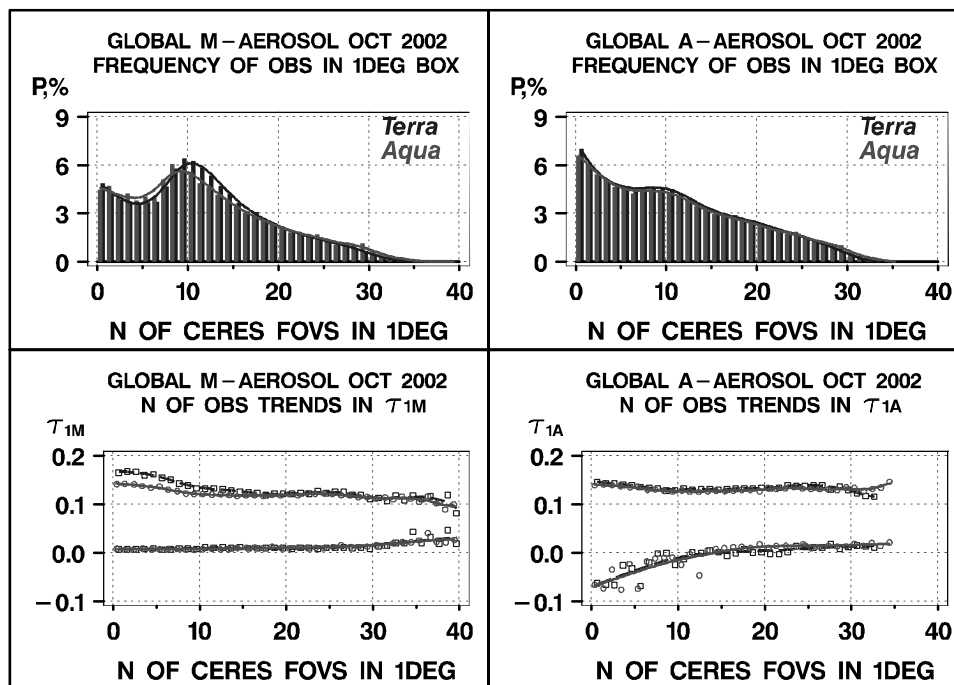


**Figure 3.** (top) Count of CERES FOVs in  $1^\circ$  boxes in the (left) M and (right) A products. (bottom) Trends in the mean and minimum AOD: (left)  $\tau_{1M}$  and (right)  $\tau_{1A}$  from Terra (squares and dashed lines) and Aqua (circles and solid lines). Note that  $\tau_{1M}$  are truncated in the M\*D04 processing and therefore  $\min(\tau_{1M})$  never goes below zero. The  $\tau_{1A}$  are not truncated and may go negative. (Physical origin of negative  $\tau_A$  is discussed by *Ignatov and Stowe* [2002b].) Trends in  $\tau_{1A}$  are smaller and more cross-platform consistent compared to  $\tau_{1M}$ . Divergence between Terra/Aqua  $\tau_{1M}$  trends at  $N < 20$  may be due to residual cloud screening differences between MOD04 and MYD04. Close agreement between  $\min(\tau_{1A})$  in MODIS band 1 from Terra and Aqua 1 indicates excellent cross-platform calibration consistency [*Ignatov, 2002*].

may also contribute to the observed differences. However, the contribution of each individual band (e.g., band 6) to the multispectral  $\tau_{1M}$  product is unknown. One of the anonymous reviewers of this paper pointed out that the less populated  $1^\circ$  areas are likely associated with near-glint areas, mainly found on the solar side of orbit. Additional correlative analyses (not shown) suggest that a larger proportion of these scarcely populated boxes (relative to the general population) indeed belong in these geometry domains. As a result, the diverging trends at  $N < 20$  (Figure 3), at glint angles  $40^\circ < \gamma < 65^\circ$  (Figure 13), and on the solar side of the orbit (Figure 10) may all be interrelated.

[33] Global average statistics of  $\tau_1$  and auxiliary parameters based on the  $(1^\circ)^2$  data are listed in the even rows of Table 1. They differ systematically from their finer-resolution CERES FOV counterparts. The global mean  $\tau_1$  derived from daily  $1^\circ$  data are all systematically higher than their CERES FOV counterparts, due to a lognormal nature of AOD density distribution (*O'Neill et al. 2000*). The  $1^\circ A_T$  averages are also larger than their CERES FOV counterparts, because the “double averaging” (first aggregating MODIS pixels into CERES footprints, and then CERES FOVs into  $1^\circ$  averages) tends to give larger weight to the cloudy areas, thus leading to a positive bias in  $A_T$  statistics derived from lower-resolution data.

[34] In the remaining part of this study, we concentrate on the analyses of  $1^\circ$  data, assuming that the effect of spatial

scale does not qualitatively alter the results of the comparisons, as long as consistent sampling and statistic (arithmetic or geometric) is used. The scale dependence of the mean global AOD values calls for better understanding and proper handling of this effect on the aerosol signals.

## 5. Global Maps and Histograms of Retrievals

### 5.1. Geographical Distribution

[35] Figure 4 shows global distributions of  $\tau_{1M}$  and  $\tau_{1A}$  from Terra or Aqua derived from  $1^\circ$  data averaged over the 9-day period. At a first glance, all four products show remarkable agreement, despite large differences in the M and A sampling and aerosol algorithms and in the Terra and Aqua orbital configurations. A closer look, however, reveals subtle yet detectable dissimilarities. The largest differences are between the M products from Terra and Aqua in the “roaring forties” of both hemispheres. The A products, on the other hand, are more consistent across platforms in area coverage, mean values of  $\tau_{1A}$ , and spatial patterns. All products show some “blurriness” around the costal lines, due to the large size of the CERES footprints [*Ignatov et al., 2005*].

[36] Regarding the M versus A comparisons, the two products are similar, but agree somewhat better for Aqua than for Terra. Differences in the application of water surface classification maps are apparent. The A product

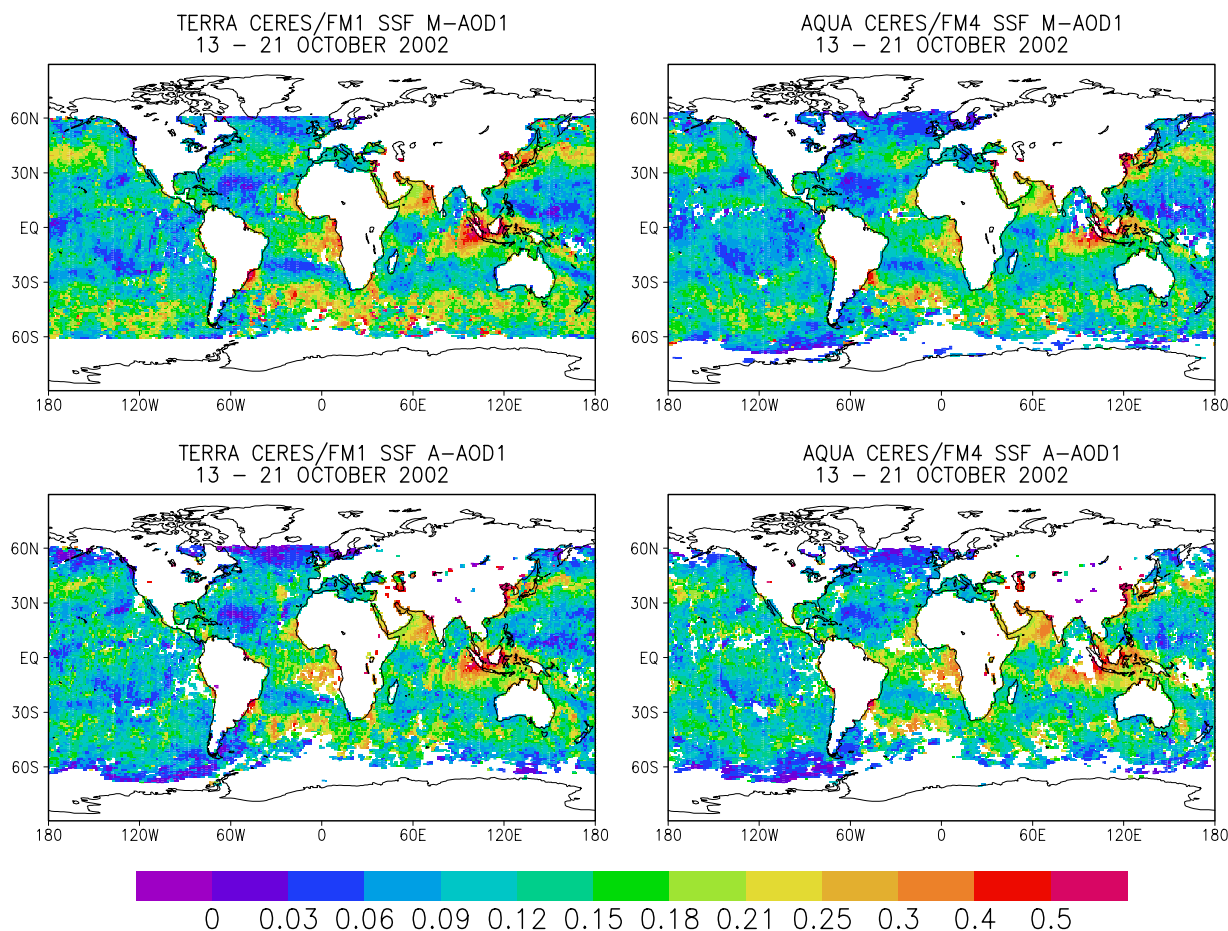


**Figure 4.** Global distribution of  $\tau_{1M}$  and  $\tau_{1A}$  derived from  $1^\circ$  Terra and Aqua data and averaged over the 9-day period from 13 to 21 October 2002.

tends to have more data points over inland water bodies, such as the Caspian Sea and Lakes Baikal and Victoria, than the M product. The M\*D04 processing does not calculate ocean aerosol in the  $(10 \text{ km})^2$  grid if even one pixel is over a land surface, whereas, the A product calculations only require the 1-km pixel being processed corresponds to a water surface. The  $\tau_{1A}$  values over inland waters, although present here, are however often unrealistic, being biased either high or low due to violations of the assumptions of the retrieval algorithm [Ignatov and Stowe, 2002a]. An example of high  $\tau_{1A}$  bias is found over the Caspian Sea. Although a relatively large value of AOD is expected over this highly polluted basin, the Caspian Seawater is also very turbid causing a bright surface reflectance that is interpreted as an elevated AOD. Collection 4 of the M\*D04 product stopped reporting aerosol retrievals over much of the Caspian Sea after adding the turbidity test [Remer et al., 2005]. (In turbid waters, top-of-atmosphere reflectances in MODIS bands 0.55, 0.66, and  $0.86 \mu\text{m}$  are biased high relative to the  $0.47$  and  $>1 \mu\text{m}$  bands, which remain largely unaffected [Li et al., 2003].) Examples of low  $\tau_{1A}$  bias are found e.g., over the two high-altitude lakes in China: the Namu ( $30^\circ\text{N}$ ,  $90^\circ\text{E}$ ,  $h \sim 4,700 \text{ m}$ ) and the Koko Nor ( $37^\circ\text{N}$ ,  $100^\circ\text{E}$ ,  $h \sim 3,200 \text{ m}$ ). The in situ Rayleigh optical depth at those altitudes is much smaller than used in the retrieval look-up tables, which were created assuming that the water

boundary is located at sea level. As a result, too much contribution is subtracted from the satellite radiance, driving the retrieved  $\tau_{1A}$  below zero with values ranging from  $-0.07$  to  $-0.05$ . Ignatov and Stowe [2002a] discuss in more detail the  $\tau_{1A}$  anomalies over bright and high-altitude inland waters.

[37] Figure 5 shows zonal sampling densities and variations in the AOD retrievals. Cross-platform differences are smaller and more spatially localized in the A product. Both products yield low values at high latitudes. These areas are generally clean and have low AOD, but they are also associated with low solar elevations and may be biased due to the increased complexity of cloud screening and possible violations of the plane-parallel assumption in the 6S radiative transfer model [Ignatov and Stowe, 2002a]. In the CERES SSF data, both the M and A retrievals are reported if  $\theta_s < 70^\circ$ . Assessment of the  $\theta_s$  bias, if any, caused by modeling inadequacies, would require sampling the same areas over the full range of the daily  $\theta_s$  cycle. This is best achieved from geostationary platforms, e.g., [Brindley and Ignatov, 2006] or using data from a satellite with a precessing orbit, such as TRMM. For satellites in near-polar orbits, the latitude and  $\theta_s$  are correlated, so it is not possible to evaluate the possible  $\theta_s$  dependency using Aqua and Terra.

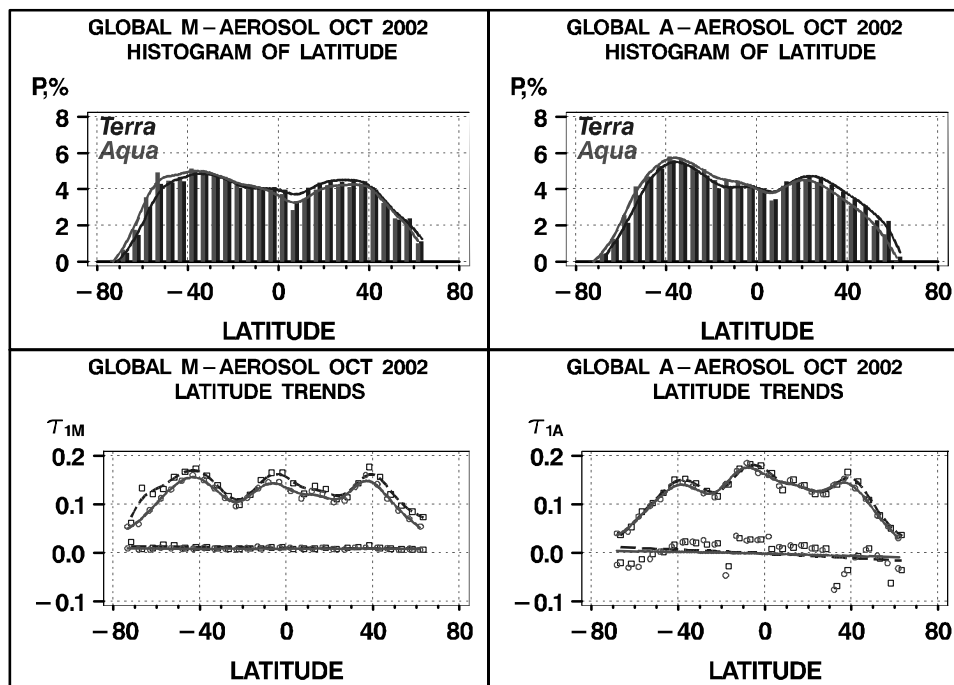


**Figure 5.** Same as in Figure 3 but for zonal density and trends in the retrievals (bin size of  $5^\circ$ ). Note that spatial coverage from Terra and Aqua is similar in both M and A products and that the A product shows more cross-platform consistency than the M product.

## 5.2. Histograms of $\tau_1$

[38] Plots of  $\tau_1$  probability density functions (PDF) derived from the  $1^\circ$  data are shown in Figure 6 (top). Their shapes are close to the lognormal distribution [O'Neill et al., 2000; Ignatov and Stowe, 2002b; Matthias and Bösenberg, 2002]. Geometric  $\tau$  statistics are also superimposed. They systematically differ from their arithmetic counterparts listed in Table 1, due to  $\tau$  lognormality. However, if a consistent statistic (arithmetic or geometric) is considered, then the mean values of  $\tau_1$  are typically within  $\sim\pm 0.01$  of each other from either M or A product and Terra or Aqua platform. According to Table 1 and Figure 6, the global mean cross-platform differences in  $\tau_{1A}$  are a factor of  $\sim 3$ – $7$  smaller than in  $\tau_{1M}$ . This result agrees with the qualitative observation from Figure 4 that the A product is more cross-platform consistent.

[39] The frequency distributions are replotted in  $\log\tau$  space at the bottom of Figure 6, which also shows their skewness ( $s$ ) and kurtosis ( $k$ ). Skewness characterizes the asymmetry of a distribution, while kurtosis provides a measure of the width relative to a normal distribution. All four PDFs show a negative skewness,  $s < 0$  (i.e., left tails are heavier than the right tails), and a positive kurtosis,  $k > 0$  (i.e., they are peaked more than a Gaussian distribution). One should not expect a perfect Gaussian fit to a nonuniform global sample of dissimilar aerosol conditions, but any additional errors in the product would deteriorate the fit. In this regard, the  $\tau_{1M}$  PDFs are closer to a lognormal shape than the  $\tau_{1A}$  PDFs: the M skewness and kurtosis are factors of 3 and 10, smaller than in their A counterparts, respectively.

## 5.3. Histograms of $\tau_1$ From the Previous SSF Release

[40] Figure 7 replots Figure 6 but using data from the previous SSF release.

[41] The new Aqua M product in Figure 6 is based on exactly same MYD04 input (collection 4), and yet, it differs from the earlier SSF release shown in Figure 7. For instance, the global geometric mean  $\tau_{1M}$  increased from 0.095 in the previous release to 0.102. Interestingly, the new Aqua  $\tau_{1M}$  deviates from a Gaussian shape more than the previous one, as manifested by the increased skewness and kurtosis. These changes are simply due to a changed mapping of the same 10-km MYD04 product into the CERES footprints (every fourth pixel instead every other pixel used earlier). On the other hand, the new Terra M product in Figure 6 is now based on MOD04 collection 4, whereas in the earlier release it was based on collection 3 data. Clearly, cross-platform consistency has significantly improved when a consistent M\*D04 collection 4 is used.

[42] The improvement in the A product is more incremental than in the M product, but it is statistically significant. The new A products agree better across platforms, and their histograms are narrower and closer to a lognormal shape. The difference between the two A products shown in Figures 6 and 7 stems from two different factors. First, a different sampling was used as discussed in section 3 above (which additionally affects the A retrievals through a more stringent spatial uniformity test in the new release). Second, values of the solar constant used in the A processing have been corrected. In the previous release, the TRMM/VIRS solar constant,  $F_o = 531.7 \text{ W m}^{-2} \text{ sr}^{-1} \mu\text{m}^{-1}$ , was mistakenly used to convert L1b radiances to reflectances for both Terra and Aqua. In the new release, the following values are used:  $F_o = 511.3$  and  $511.9 \text{ W m}^{-2} \text{ sr}^{-1} \mu\text{m}^{-1}$  for Terra and

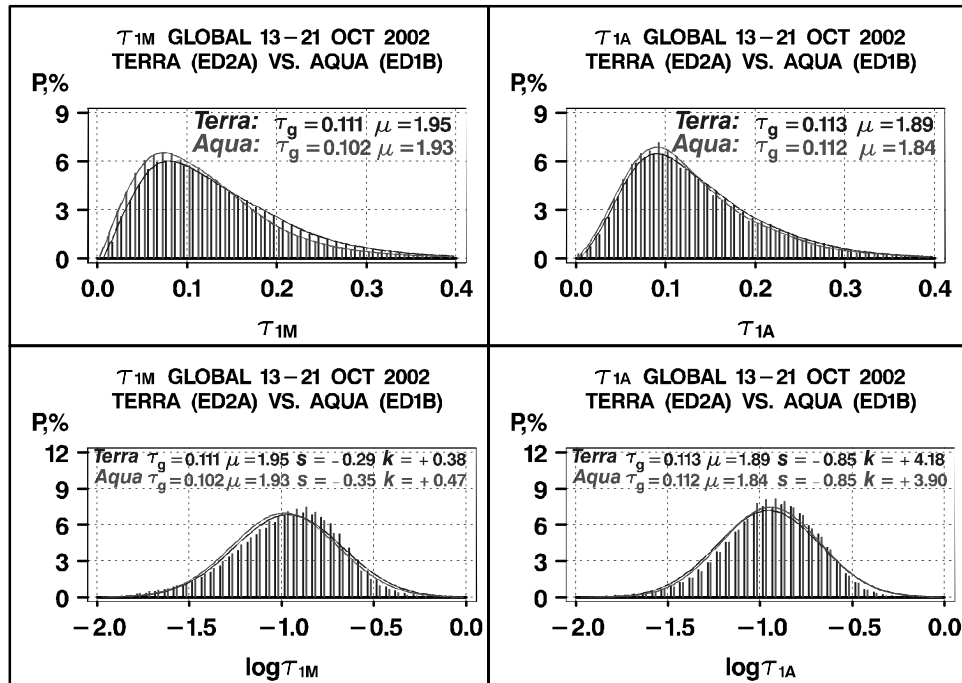


**Figure 6.** (top) Histograms of  $\tau_{1M}$  and  $\tau_{1A}$  derived from the current release CERES SSF 1° Terra (edition 2A) and Aqua (edition 1B) global data from 13 to 21 October 2002. Geometric mean and STD statistics are superimposed. (bottom) Same but for  $\log(\tau_{1M})$  and  $\log(\tau_{1A})$ . In addition to geometric mean and STD statistics, skewness ( $s$ ) and kurtosis ( $k$ ) are also shown. (Note that for a Gaussian distribution,  $s = k = 0$ .)

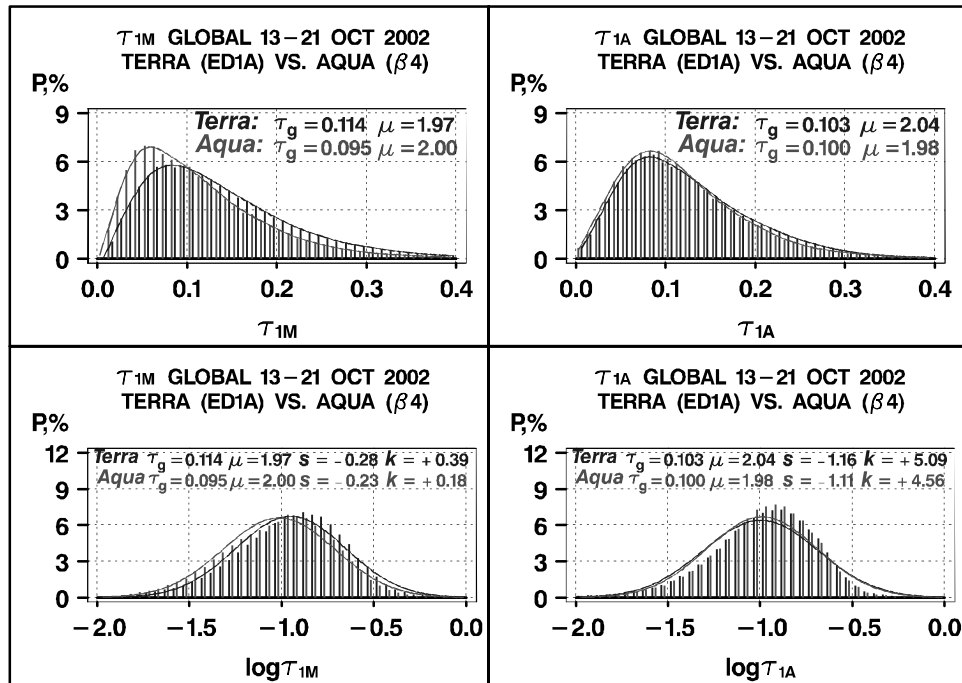


**Figure 7.** Same as in Figure 6 but using data from the previous SSF release, which employed the same aerosol algorithms but different M and A preprocessing and sampling. In particular, the Terra M product was based on MOD04 collection 3 (the latest release shown in Figure 6 is based on collection 4). The SSF processing is based on 1-km data subsampled in every second column and every second row (the current release shown in Figure 6 subsamples every fourth pixel in every second row.) Also a ~4% solar flux error in the A product was fixed in the latest SSF release. See section 4 for further discussion.

Aqua, respectively. This 4% reduction in the solar constants, which is indistinguishable from a calibration change, effectively raised the Terra and Aqua reflectances in the new release by +4% from the previous release. According to Ignatov [2002], the effect of a calibration change on the retrieved AOD at  $0.63 \mu\text{m}$  is estimated as  $\Delta\tau_{1A} \sim (0.37 + 0.71\tau_{1A})\varepsilon_1$ . For typical AOD over ocean with modal value of  $\tau_{1A} \sim 0.1$  and error  $\varepsilon_1 \sim +0.04$ , the expected average increase in  $\tau_{1A}$  is  $\Delta\tau_{1A} \sim +0.02$ . However, note that the new  $\tau_{1A}$  modal values in Figure 6 are only  $\sim+0.01$  larger than the old numbers in Figure 7. This is because about half of the expected calibration-induced  $\tau_{1A}$  change was effectively offset by a more stringent spatial uniformity test in the new SSF release. The effect of cloud screening on AOD is further discussed in section 6.1 below.

[43] These examples clearly show the importance of using an objective and consistent sampling to ensure the quality of a given aerosol product, especially when it is part of a climate data record. We also emphasize the value of the simple consistency checks, which were employed here to successfully capture subtle changes in the AOD product without resorting to complex and time-consuming validation against ground based Sun photometers. Validation is often considered the ultimate measure of product accuracy, and rightly so. On the other hand, it may fail to capture subtle product differences because the number of validation samples is often limited and large uncertainties are introduced by spatial-temporal mismatch between the satellite and ground data. Using the two techniques in concert is deemed to improve the quality control of satellite retrievals.

## 6. Cloud Amount and Angular Dependencies of Retrievals

[44] The data in Table 1 show that some auxiliary parameters, cloud amounts and viewing and illumination angles, associated with the retrievals systematically differ between the products and platforms. These differences may affect the products, if the retrieval algorithm performs nonuniformly over the full range of cloud conditions and retrieval geometry. In this section, these cross-platform and cross-product differences in the retrieval domains and their effect on aerosol retrievals are analyzed. The relationships between a given auxiliary parameter and AOD are estimated using only one week of data and therefore may be distorted by possibly misleading false correlations between different factors, which are not fully independent (for instance, low  $\tau_{1M}$  and  $\tau_{1A}$  at high Sun  $\theta_S > 50^\circ$  may come from clean high latitudes). Until a more representative data set is used for analyses of such dependencies, we concentrate here on the comparison of domains in which retrievals are available in the two products and from the two platforms. The focus is on the cross-platform consistency in the dependence of AOD on a given parameter when false correlations (if present) are expected to be minimized. Note that similar comparisons between the M and A products should also be deferred until the large differences in their respective samplings are resolved.

### 6.1. Cloud-Aerosol Correlations

[45] Figure 8 plots histograms of  $A_T$  and the variations of  $\tau_1$  with  $A_T$ . Note that the ambient cloud amount

measured by  $A_T$ , should be a good proxy for subpixel cloud contamination.

[46] The two major features in Figure 8 are that the relative proportion of “aerosol burden”  $1^\circ$  grids decreases with  $A_T$  in the A product but increases in the M product, and that  $\tau_1$  increases with ambient cloud amount in all four products. Both features have been previously observed in the AVHRR, VIRS and Terra/MODIS data [Ignatov *et al.*, 2005, and references therein]. This study mainly focuses on cross-platform, cross-product, and cross-version consistency of these features.

[47] The increased frequency of M pixels at larger  $A_T$  seems counterintuitive and maybe due to the uncertainty in the CERES-derived  $A_T$  value. Some regions with large  $A_T$  may actually be misidentified as clouds by the more conservative CERES cloud mask but correctly identified as aerosols by the M\*D04 processing. (For instance, the A panels in Figure 4 (bottom) show more missing data in the center of the Saharan dust outbreak compared to the M panels (Figure 4, top).) Or, boxes with large  $A_T$  may be correctly identified as cloud by the A processing but misidentified as aerosol by the less conservative M processing. (Such a scenario might take place in some areas of the “roaring forties”.) The relative success/failure rate of the M and A cloud masks may vary from one geographical area or season to another, and more analyses are needed to more fully evaluate the relative performance of the two cloud masks.

[48] The  $\tau_1(A_T)$  trends compare better across platforms for the same product than across products from the same platform. (For instance, the slope of  $\tau_1(A_T)$  is a factor of  $\sim 2$  smaller in the  $\tau_{1A}$  than in  $\tau_{1M}$ .) This is consistent with the data in Table 1, which show that  $A_T$  differences are smaller across platform than across product. Table 1 further shows that the CERES cloud mask is more conservative than the M\*D04 mask ( $A_T \sim 31\%$  in the A product versus  $A_T \sim 47\%$  in the M product).

[49] At least part of the  $\tau_1(A_T)$  correlations may be due to real cloud-aerosol interactions. However, the fact that  $\tau_{1M}(A_T)$  diverges between Terra and Aqua at large  $A_T$  (or at small N in Figure 3) indicates that the effect of subpixel cloud is present. Some actual morning-afternoon differences between the  $\tau$  and  $A_T$  from the two platforms may exist, due to the 3-hour time lag. However, the  $\tau_1(A_T)$  relationship is expected to hold from platform to platform, at least for the same product. Recall that many of the current cloud screening procedures (including those used in the M and A aerosol production) are threshold-based and have difficulty resolving subpixel clouds, a problem that is deemed to be a continuous rather than a discrete process.

[50] Figure 9 replots Figure 8 but using data from the previous SSF release. Clearly, the cross-platform consistency between the Terra M product has improved in the new release, which manifests itself in both more consistent  $A_T$  histograms and  $\tau_{1M}(A_T)$  variations. The changes in the A product are twofold. First, as a result of a more stringent spatial uniformity test, the drop-off in the  $A_T$  histograms starts at  $\sim 60\%$  in the new release compared with  $\sim 75\%$  in the previous release. Apparently, this change has reduced the proportion of CERES FOVs at high-end  $A_T$  but it has not affected the  $\tau_{1A}(A_T)$  behavior. The other difference is that the new  $\tau_{1A}$  has increased by  $\sim 0.02$  at  $A_T$  near 0%.

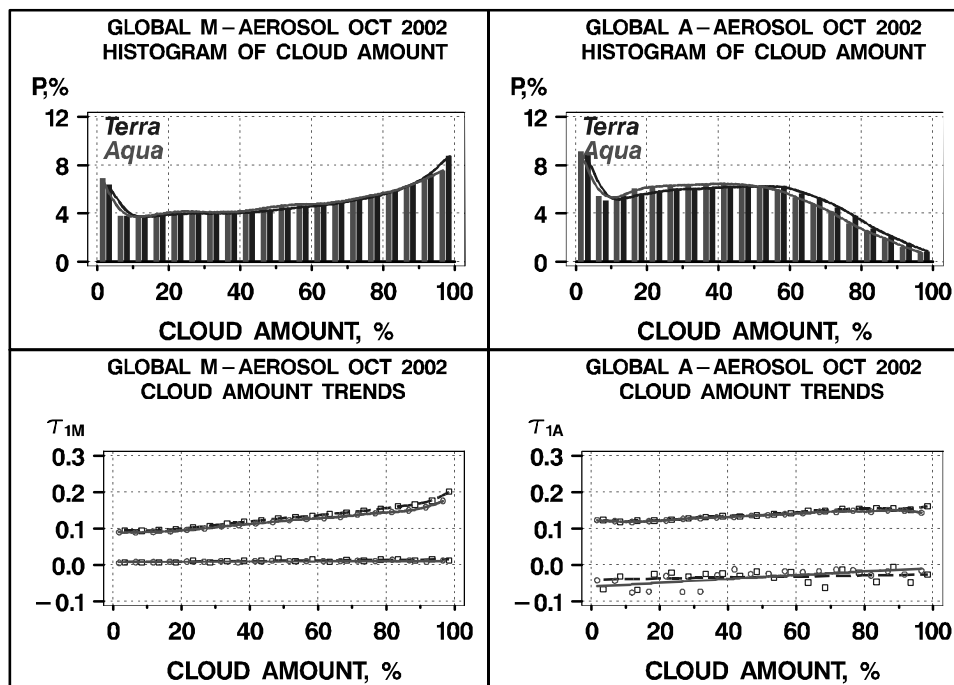


**Figure 8.** Same as in Figure 3 but for the ambient cloud amount,  $A_T$  (binned at  $\Delta A_T = 5\%$ ). Note that  $A_T$  was determined by the A cloud screening. For the exact definition of  $A_T$  and for relevant discussion, see section 4.1. In the M product, maximum of the  $A_T$  histograms is found in the highest bin centered at  $A_T \sim 97.5\%$  (includes data with  $95 \leq A_T < 100\%$ ), whereas in the A product, it is in the lowest bin at  $A_T \sim 2.5\%$  (includes data with  $0 \leq A_T < 5\%$ ). The average  $A_T$  is  $\sim 47\%$  in the M products compared to  $A_T \sim 32\%$  in the A product (see data in Table 1). The  $\tau_{1A}$  trends are smaller compared with  $\tau_{1M}$  trends and more reproducible cross platform. Small divergence between the two  $\tau_{1M}$  trends toward larger  $A_T$  values may indicate residual cloud-screening differences in the M product between the two platforms (see  $\tau_{1M}(N)$  trends in Figure 3).

This change is due to eliminating the error in the solar constants discussed in section 5.2.

## 6.2. Dependence on Viewing and Illumination Geometry

[51] Figures 10–13 show histograms (Figures 10 (top) to 13 (top)) of viewing zenith (VZA;  $\theta_V$ ), solar zenith (SZA;  $\theta_S$ ), scattering ( $\chi$ ), and glint ( $\gamma$ ) angles, and AODs (Figures 10 (bottom) to 13 (bottom)), as functions of the same angles. Note that VZA is defined as negative on the solar side of the orbit and positive on the antisolar side.

[52] The retrievals are made in different angle domains in the two products and from the two platforms. Neither algorithm retrieves AOD within  $40^\circ$  of the glint angle around the specular point resulting in dips in their respective  $\theta_V$  histograms around nadir (Figure 10) and truncation of the high Sun angles in the  $\theta_S$  histograms (Figure 11). In addition, the A algorithm historically is not applied when  $\theta_{VA} > 60^\circ$  and on the solar side of the orbit ( $\theta_{VA} \leq 0^\circ$ ), whereas the M technique allows  $\tau_M$  retrievals up to the scan edge on both sides of the orbit ( $-66^\circ \leq \theta_{VM} \leq 66^\circ$ ). Aqua makes its retrievals at slightly larger SZAs (Figure 11), and, in the M product, over a smaller range of SZAs. These differences in the ranges of SZAs between the algorithms arises from the VZA limitations seen in Figure 10. The large

differences in the SZA domains for the two products significantly exceed cross-platform differences.

[53] Variations of AOD compare generally well across platform in both products, but develop cross-platform biases in certain domains of retrieval geometry. In particular,  $\tau_{1M}(\theta_V)$  diverges on the solar side of the orbit by  $\sim 0.03$ , whereas  $\tau_{1A}(\theta_V)$  shows a  $\sim 0.02$  anomaly in the vicinity of  $\theta_V \sim 20^\circ$  (Figure 10). The  $\tau_{1M}(\theta_S)$  variations are coherent, but biased by  $\sim 0.01$  over the full range of SZA, whereas  $\tau_{1A}(\theta_S)$  behaves similarly for both platforms except under a very high Sun ( $\theta_S < 35^\circ$ ). Both products decline at large SZAs ( $\theta_S > 50^\circ$ ). Part of this effect maybe due to a false correlation (aerosol loading is generally lower in the remote high-latitude areas), and part may be due to the increased retrieval biases at low Sun elevations [Ignatov and Stowe, 2002a].

[54] The  $\tau_1(\chi)$  variations with scattering angle (Figure 12) are largely consistent in both products, whereas the glint angle behavior of  $\tau_{1A}(\gamma)$  shows some cross-platform biases at high glint angles  $\gamma > 95\text{--}100^\circ$ . In addition, the  $\tau_{1M}$  values differ by as much as 0.02 when  $\gamma < 65^\circ$ .

[55] Overall, the analyses in this section reveal the effects of large sampling differences in the two products. Cross-platform inconsistencies are generally larger in the M product. Note that these results are based on a limited time domain. To cover a larger range of solar and scattering

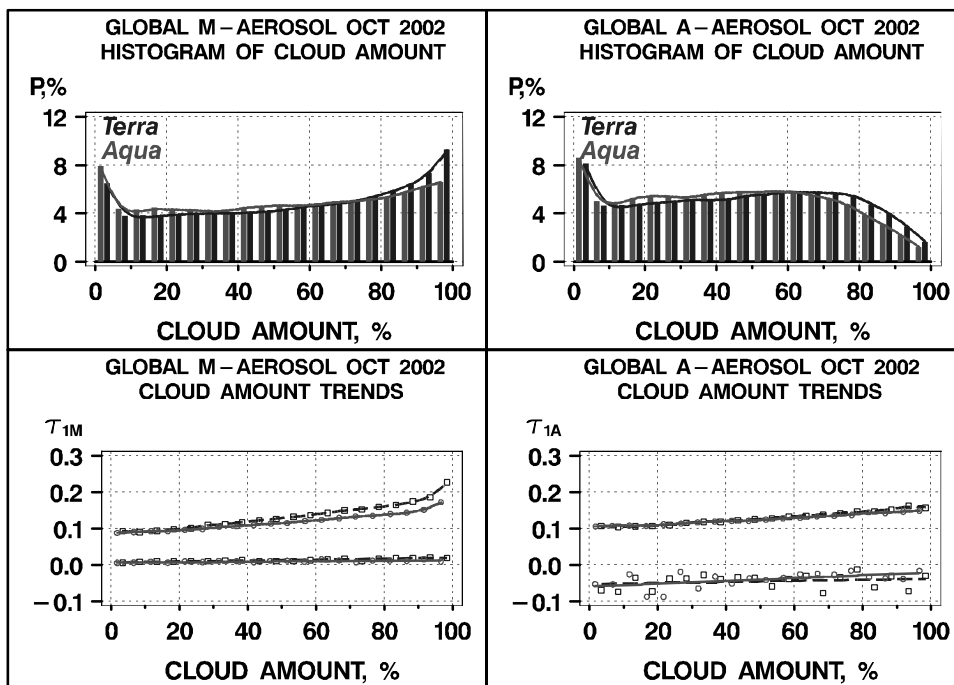


**Figure 9.** Same as in Figure 8 but using data from the previous SSF release (see caption to Figure 7 for more detail on the release difference). Note the following differences with the previous release: (1) Cross-platform differences in the M product are larger than in Figure 8 (see histograms and  $\tau_{1M}(A_T)$  trends at large  $A_T$ ). (2) The A histograms extend further into large  $A_T$  domain and are less cross-platform consistent than in Figure 8. (3)  $\tau_{1A}$  at  $A_T \sim 0\%$  is  $\sim 0.02$  smaller than in Figure 8.

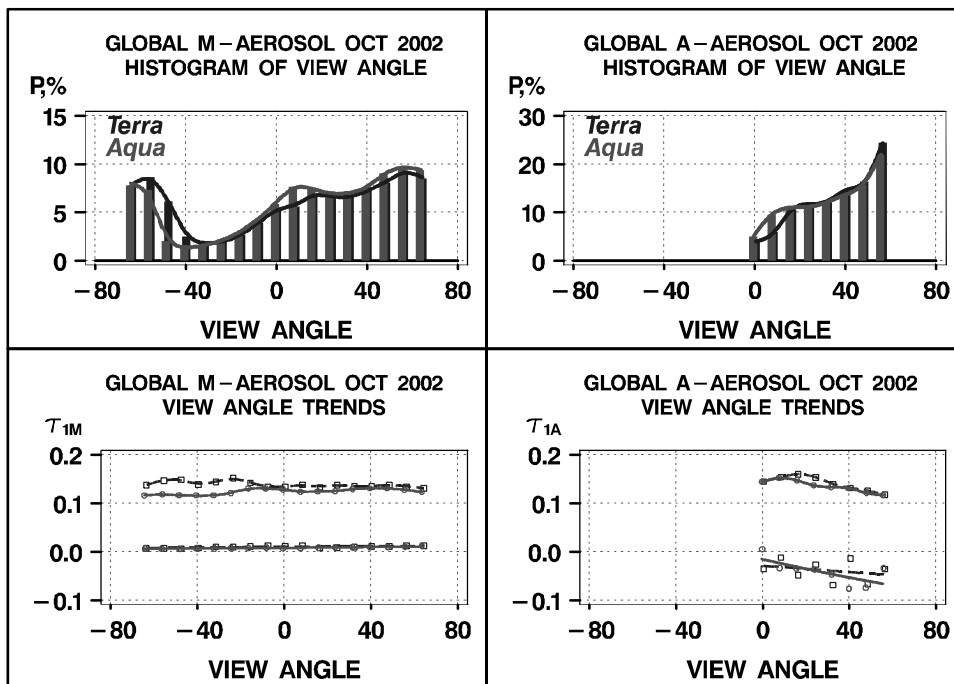


**Figure 10.** (top) Histograms of view angle in (left) M and (right) A products (bin size  $\Delta\theta_V = 8^\circ$ ). Note that view angle is defined as negative on the solar side of orbit and positive on the antisolar side. View angle domains from Terra and Aqua are similar but differ between M and A products. (bottom) View angle trends in  $\tau_{1M}$  and  $\tau_{1A}$ . Note that the A product is more cross-platform consistent than the M product, which develops cross-platform differences on the solar side of orbit. Note that these differences cannot be observed if no differentiation is made between the solar and antisolar sides as by, for example, Ichoku et al. [2005].

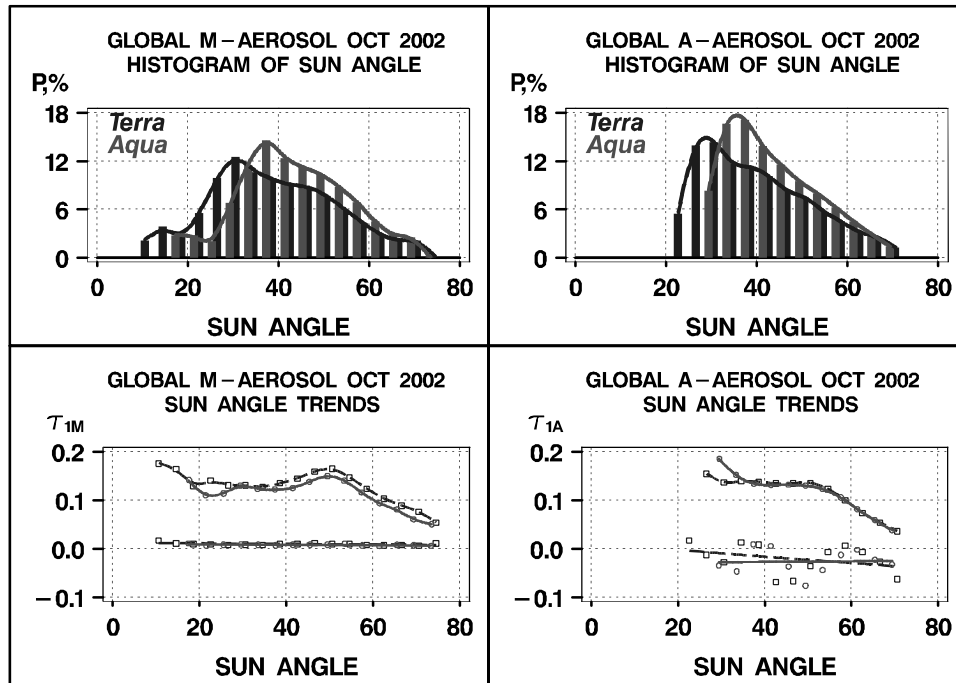


**Figure 11.** Same as in Figure 10 but for the solar zenith angle (bin size  $\Delta\theta_S = 5^\circ$ ). Retrievals from Aqua are made at a lower Sun than from Terra. Range of Sun angle is wider in M than in A products. Trends in  $\tau_{1M}$  are cross-platform consistent, but the curves are systematically shifted by  $\sim 0.01$ . The  $\tau_{1A}$  trends are consistent except at very high Sun ( $<35^\circ$ ). Low bias in  $\tau_{1M}$  and  $\tau_{1A}$  at Sun angle ( $>50^\circ$ ) maybe due to correlation with geography (high-latitude clean open ocean areas) or increased cloud screening difficulties and violation of plane parallel radiative transfer assumption used in 6S.

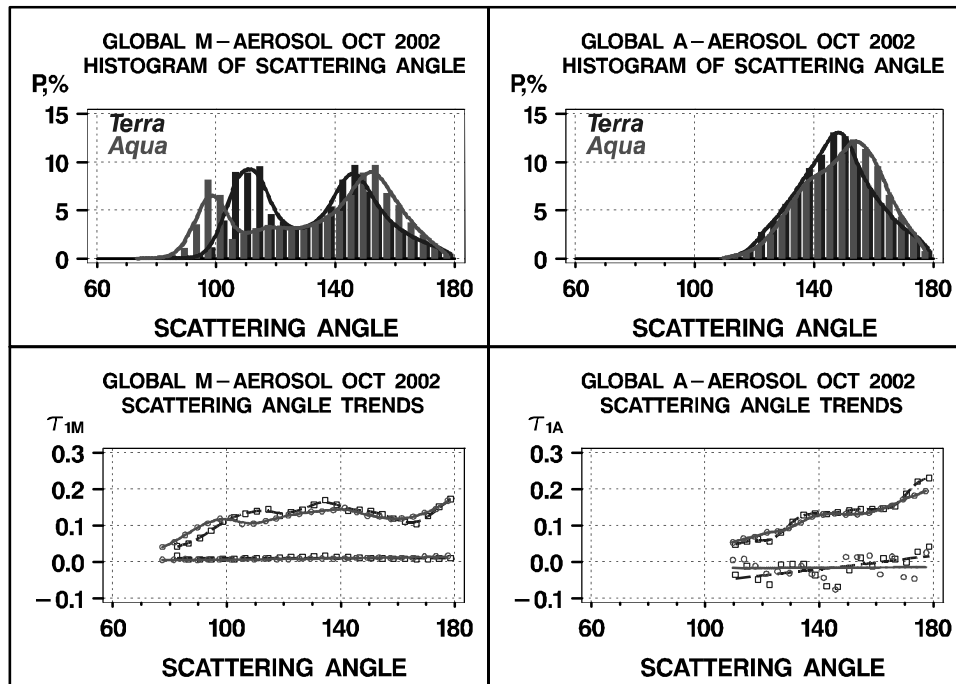


**Figure 12.** Same as in Figure 10 but for the scattering angle (bin size  $\Delta\chi = 5^\circ$ ). Retrieval domains from Aqua and Terra are close, with Aqua being slightly shifted toward backscatter. Range of scattering angle is wider in the M than in the A product. Trends in  $\tau_{1M}$  are cross-platform consistent in both products and larger in the A product. Part of trends may be due to correlation with geography.

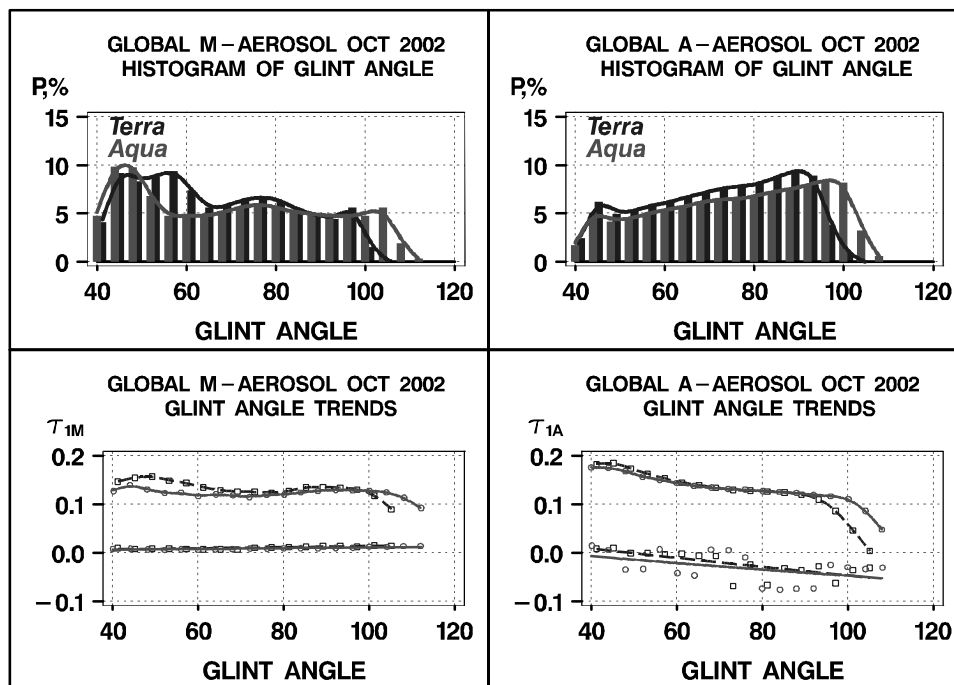


**Figure 13.** Same as in Figure 10 but for the glint angle (bin size  $\Delta\gamma = 5^\circ$ ). Note that in both products, retrievals are not made at  $\gamma < 40^\circ$ . Retrieval domains from Aqua and Terra are close with Aqua being further away from the glint area. Range of glint angle is wider in the M than in the A product. Both products diverge at  $\gamma > 90$ – $100^\circ$ , and the M product additionally diverges at  $40^\circ < \gamma < 65^\circ$ .

angles and to ensure that these results are representative, a data set covering other months should be analyzed in the future.

## 7. Refined Space-Time Matchup in the Product Comparisons

[56] At least a part of the cross-platform and cross-product  $\tau_1$  difference is due to the sampling differences since no attempt was made to precisely match the  $\tau_1$  data in space and time. For the analyses in this section, the  $1^\circ$  data from Terra and Aqua for both products have been merged by latitude, longitude, and day to form the respective matchup data sets. The respective four matchup data sets are defined as those containing the following [ $1^\circ$ -1 day] boxes in which (1) the M product is available from both satellites (M Terra/Aqua intersection), (2) the A product is available from both satellites (A Terra/Aqua intersection), (3) both M and A products are available from Terra (Terra A/M intersection), and (4) both M and A products are available from Aqua (Aqua A/M intersection). Two comments should be made before we proceed with the analyses of the matchup data sets below.

[57] First, the time difference between Terra and Aqua remains and may affect results of cross-platform comparisons using the Terra/Aqua matchup data sets (both M and A) in section 7.1. Additionally, spatial noise is also present in all four matchup files, as the  $1^\circ$   $\tau_1$  averages actually come from different parts of the  $1^\circ$  box and may be separated by up to 150 km. It affects the comparison statistics in sections 7.1 and 7.2. Quantifying the effect of spatial and temporal noise on the results of comparisons is a complex task that is

outside the scope of this study. Instead, the focus is on the relative, rather than absolute, comparison statistics (correlation coefficient,  $R$ ; bias,  $\delta$ ; and noise,  $\sigma$ ), which are equally affected by the spatiotemporal mismatch errors.

[58] Second, the matchup data sets are subsamples of the full data set. For its statistics to hold over the full sample, the matchup must be representative of the full sample. A simple check of representativeness is required but often overlooked. For instance, validation statistics obtained from comparison with a limited number of Sun photometers, mostly in the coastal tropical areas, is assumed to represent the performance of the global satellite product, but this assumption is never checked [e.g., Ignatov et al., 1995; Remer et al., 2002, 2005; Myhre et al., 2004]. This question is further discussed in section 7.3.

### 7.1. Cross-Platform Comparisons: Terra Versus Aqua

[59] Cross-platform comparisons are useful to determine if the AOD is captured consistently from the two platforms. Table 2 shows that the M product is available from both Terra and Aqua in 96,275 [ $1$  day- $1^\circ$ ] boxes, whereas the A product is available from both platforms in only 29,742 boxes. These two subsamples of the full M and A products are termed the M and A Terra/Aqua intersections, respectively. Figures 14a and 14b plot “ $\tau_{\text{TERRA}}$  versus  $\tau_{\text{AQUA}}$ ” scattergrams from these two intersections. Cross-platform noise appears to be larger in the M product. The respective correlation coefficients are also superimposed:  $R = 0.73$  in the M and 0.80 in the A product.

[60] Data points in the “ $\tau$  versus  $\tau$ ” scattergrams are very nonuniformly distributed. The vast majority of points are found in the first quadrant close to the origin. Taking into

**Table 2.** Global Mean Statistics of  $\tau_{1M}$  and  $\tau_{1A}$  and Auxiliary Parameters in the M and A Terra/Aqua Intersection Data Sets From 13 to 21 October 2002

Terra/Aqua M	N	$\tau_{1M}$	LT, hours	$A_T$ , %	$\theta_v$ , deg	$\theta_s$ , deg	$\chi$ , deg	$\gamma$ , deg
Terra	96,275	0.132	10.45	53.3	5.4	39.9	130.2	63.6
Aqua	96,275	0.121	13.64	51.9	9.2	44.8	132.2	67.1
Terra/Aqua A	N	$\tau_{1A}$	LT, hours	$A_T$ , %	$\theta_v$ , deg	$\theta_s$ , deg	$\chi$ , deg	$\gamma$ , deg
Terra	29,742	0.124	10.07	38.1	36.6	40.4	145.6	69.3
Aqua	29,742	0.120	13.97	35.7	34.2	45.3	148.2	74.1

account  $\tau$  lognormality, Figures 14c and 14d replot the “ $\tau$ - $\tau$ ” scattergrams as “ $\log\tau$ - $\log\tau$ ”. The clusters are better constrained in a log space. (Note that the A log sample is reduced, because logarithm cannot be taken of 157 non-positive  $\tau_{1A}$ , in either data set, whereas the M log sample remains unchanged because all  $\tau_{1M} > 0$ .) Interestingly, the log transformation improves correlation in the M product from  $R = 0.73$  to 0.76 (presumably due to a better constrained scatter in  $\log\tau$  space at large  $\tau$ ), whereas in the A product, the correlation actually drops from  $R = 0.80$  to 0.78 (probably due to the increase scatter at low  $\tau$ , where  $\tau$  errors are amplified when taking the logarithm). In either scale, the cross-platform correlation is larger for the A product.

[61] Figures 14e–14h plot histograms of the Terra-Aqua  $\tau$  and  $\log\tau$  differences. The A product shows a smaller cross-platform bias ( $\delta = 0.003$  versus 0.011) and noise ( $\sigma = 0.048$  versus 0.066) compared to the M product, and continues to be more cross-platform consistent, in both linear and log metrics.

## 7.2. Cross-Product Comparisons: A Versus M

[62] Ignatov *et al.* [2005] used the MA intersection to highlight the M-A aerosol algorithm differences. The sampling differences are minimized here compared to the full M and A samples but not removed completely. (For instance, Table 3 shows that the average cloud amount in the MA intersection is still higher in the M product than in the A product:  $A_T = 46\%$  versus 41% for Terra, and 45% versus 40% for Aqua.)

[63] Table 3 shows that there are 79,209 data points in which both products are available from Terra, and 77,262 such data points from Aqua, and Figure 15 plots the results of cross-product comparisons. The M-A correlation is  $R \sim 0.86$ –0.87 (an improvement from Terra edition 1A data where it was  $R \sim 0.84$  and 0.78 in December 2000 and June 2001, respectively). Cross-product scattergrams are more constrained in log space, although the correlation is somewhat reduced. The two products show a systematic bias of  $\delta \equiv (\tau_{1A} - \tau_{1M}) = 0.012 \pm 0.001$  and noise  $\sigma = 0.042 \pm 0.003$ . The M-A biases in the new SSF release are larger than the differences observed in the previous Terra edition 1A MA comparisons in December 2000 and June 2001, where they were  $\delta \sim (4 \pm 5) \times 10^{-3}$  [Ignatov *et al.*, 2005]. The results in Figure 15 suggest that for the Aqua data, the cross-product correlation is slightly greater than for Terra and the noise is smaller, but the bias is somewhat larger.

## 7.3. Statistical Representativeness of the Intersection Subsamples

[64] In matching the two data sets as closely as possible in space and time, the intersection subsample should remain

representative of both full data sets that are being compared. If the condition of statistical representativeness is not met, then the results of comparison (“validation statistics”) cannot be extended to represent the full products.

[65] For example, comparison of Table 2 with the respective 1<sup>o</sup> rows in Table 1 shows that the size of the Terra/Aqua M intersection subsample is only 60% of the full Terra or Aqua M sample, whereas the size of the Terra/Aqua A

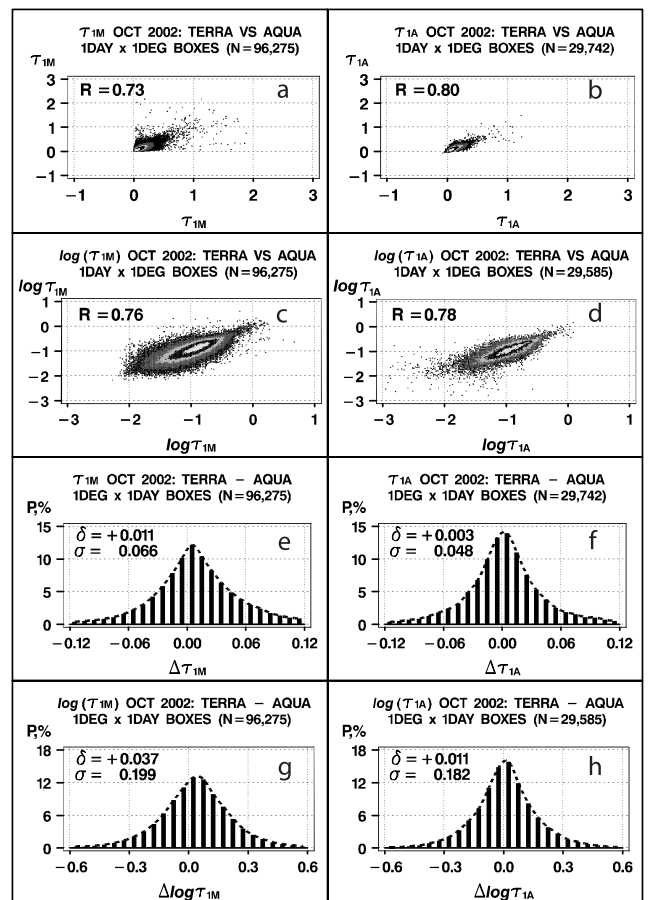


**Figure 14.** Cross-platform analyses of  $\tau_{1M}$  and  $\tau_{1A}$  derived from 1<sup>o</sup> Terra-Aqua matchup data sets (see statistics in Table 2): (a) scattergram of Terra  $\tau_{1M}$  versus Aqua  $\tau_{1M}$  (correlation coefficient,  $R$ , superimposed), (b) same as Figure 14a but for  $\tau_{1A}$ , (c and d) same as Figures 14a and 14b but for  $\log\tau_1$ , (e) histogram of Terra-Aqua  $\tau_{1M}$  difference (mean,  $\delta$ , and STD,  $\sigma$ , statistics are superimposed), (f) same as Figure 14e but for  $\tau_{1A}$ , and (g and h) same as Figures 14e and 14f but for  $\log\tau_1$ . Note that  $\tau_{1A}$  shows higher cross-platform correlation and smaller bias and RMSD.

**Table 3.** Global Mean Statistics of  $\tau_{1M}$  and  $\tau_{1A}$  and Auxiliary Parameters in the MA Intersection Data Sets for Terra and Aqua From 13 to 21 October 2002

	N	$\tau_{1M}/\tau_{1A}$	LT, h	$A_T$ , %	$\theta_V$ , °	$\theta_S$ , °	$\chi$ , °	$\gamma$ , °
MA Terra								
M	79,209	0.123	10.17	46.4	30.5	39.0	144.7	67.6
A	79,209	0.134	10.07	41.1	36.9	39.4	146.8	69.3
MA Aqua								
M	77,262	0.118	13.92	44.9	29.8	43.7	147.9	72.1
A	77,262	0.131	14.00	39.4	34.8	44.1	150.2	74.2

intersection is only  $\sim 37\%$  of the full Terra or Aqua A sample, respectively. The respective statistics of retrievals and auxiliary parameters also differ: in the intersection sample, for instance,  $A_T$  is smaller by  $\sim 3\text{--}4\%$  than in the full M and A samples. A somewhat lower cloud amount is intuitively expected in the Terra/Aqua intersection subsample, because the requirement that a  $1^\circ$  box contains at least one cloud-free MODIS pixel from both platforms is more restrictive than the requirement that it is available from at least one platform. Angular domains also differ slightly yet systematically between the full samples and matchup data sets. As a result,  $\tau_{1M}$  is smaller in the intersection subsample by  $\sim 0.005$ , and  $\tau_{1A}$  by  $\sim 0.011$  compared to the full samples. On the basis of these estimates, the Terra/Aqua differences obtained from the intersection subsamples and shown in Figure 14, are probably going to be larger if the full product is considered. The extension of the Terra/Aqua matchup statistics to the full sample is less justifiable in the A product where the full and subsampled statistics differ more significantly than in the M product.

[66] The differences between the full sample and its matchup subset are also seen by comparing the statistics of MA intersections in Table 3 with the full samples in Table 1. Typically, the MA intersection is  $\sim 96\text{--}97\%$  of the full A product but only  $\sim 48\text{--}52\%$  of the full M product. The statistics of retrievals and auxiliary parameters in the MA intersection are very close for the A product but significantly differ for the M product (average  $\tau_{1M} = 0.133$  in the full set versus only  $\tau_{1M} = 0.123$  in the intersection, cloud amounts are 55% versus 46%, etc). Therefore extending statistical conclusions obtained in the MA intersection to the full M sample is less justified than to the full A sample.

[67] The requirement of statistical representativeness is important in many remote sensing applications such as e.g., the validation of satellite products against ground-based Sun photometers. It is often overlooked that the comparisons are done in a relatively small matchup data set in which both satellite and ground-based data are available. Such matchup data sets are typically more constrained geographically than the global Terra/Aqua or MA intersection samples considered above. Also, the matchup data set maybe biased toward clear sky (being “double cloud cleared”) and continental atmospheric and surface conditions (if coastal Sun photometers are used). As a result, one may expect larger differences between the global and local matchup validation statistics than between the two global products discussed above, raising questions about its representativeness of the global satellite product. Certain regions and seasons available in the satellite product are never covered by local

ground-based measurements (e.g., many areas in the open ocean, especially in the high latitudes). On the other hand, there may be domains of Sun photometer measurements that are never observed from a satellite, due e.g., to their cloud screening differences. Analyses in this section have demonstrated that it is relatively easy to check the statistical equivalency of the intersection subsample and full data set. However, as of the time of this writing, we are not aware of any validation studies in which such checks were attempted for surface-satellite comparisons.

## 8. Conclusion

[68] This study compared global aerosol optical depth over ocean products derived from Terra and Aqua using two different sampling and aerosol algorithms. Data of two successive releases of CERES SSF data were used in the analyses, to check the evolution of the products. The results

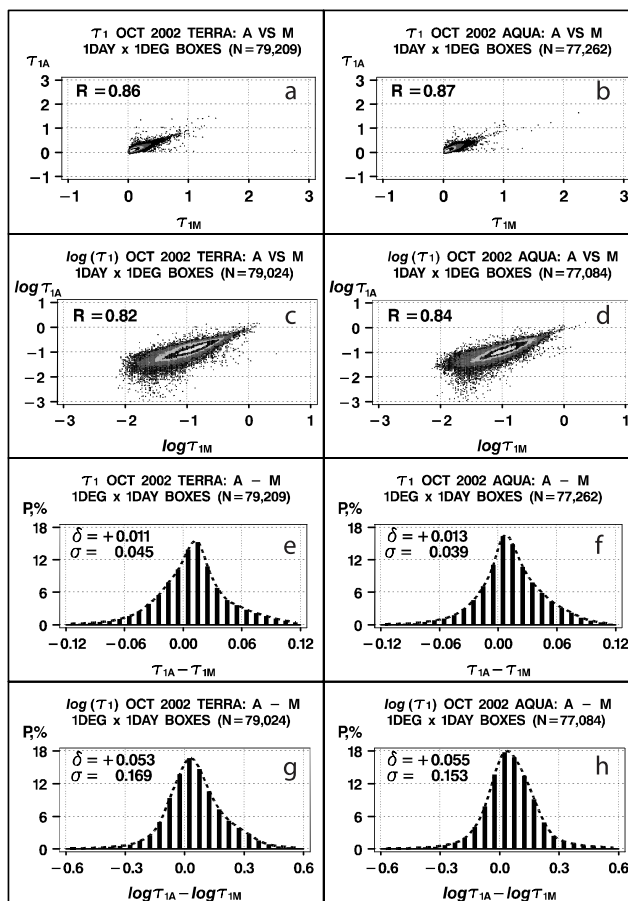


**Figure 15.** Cross-product analyses of  $\tau_{1M}$  and  $\tau_{1A}$  derived from  $1^\circ$  Terra-Aqua matchup data sets (see statistics in Table 3): (a) scattergram of  $\tau_{1A}$  versus  $\tau_{1M}$  for Terra (correlation coefficient,  $R$ , superimposed), (b) same as Figure 15a but for Aqua, (c and d) same as Figures 15a and 15b but for  $\log\tau_1$ , (e) histogram of  $\tau_{1A} - \tau_{1M}$  difference for Terra (mean,  $\delta$ , and STD,  $\sigma$ , statistics are superimposed), (f) same as Figure 15e but for Aqua, and (g and h) same as Figures 15e and 15f but for  $\log\tau_1$ . Note that  $\tau_{1A}$  shows higher cross-platform correlation and smaller bias and RMSD.

shed additional light on the current status of aerosol retrievals and highlight outstanding issues.

[69] All aerosol products show a remarkable cross-platform and cross-product consistency, and have improved in the latest SSF release. The improvement in the M product stems from using collection 4 of M\*D04 product, and the improvement in the A product is due to fixing the solar constant values that were erroneously used from *TRMM/VIRS* in the former release. Also, the A sampling has changed, but this does not appear to have any effect on the quality of the A product, except that the size of the A sample is now reduced due to the more conservative A cloud screening.

[70] The Terra-Aqua M differences have been reduced in M\*D04 collection 4, but still, they are larger than the A differences in the latest SSF release. The contrast is statistically significant and increases in less populated and cloudy areas, in the vicinity of glint and on the solar side of orbit. This suggests that residual cloud and glint screening differences between MOD04 and MYD04 are the likely cause rather than diurnal changes in aerosol abundance between Terra and Aqua overpass time. In the MOD04 collection 3, these artifacts were larger.

[71] The increased cross-platform noise in the M product indicates that generally the M\*D04 product is noisier than the CERES cloud-screened, single-channel A product. Better cross-platform consistency in the A product may be due to a more conservative and cross-platform consistent cloud screening as well as a more restricted view zenith angle range. Another factor, which may possibly contribute, is increased noise in the retrieved M aerosol model, especially at typical (low) aerosol loading over ocean. Using the nonvariable global aerosol model in the A product may be a more robust approach, which eventually results in less noisy aerosol optical depth [e.g., *Ignatov and Stowe, 2002b*]. Including the solar side of orbit in the M product adds to the observed cross-platform differences.

[72] The M and A products are highly cross-correlated, on both platforms. Generally, the A algorithm tends to retrieve larger aerosol optical depth. However, as much as half of the resulting aerosol algorithm-induced bias is offset by a more conservative cloud and glint screening in the A product. Complex compensation mechanisms between sampling and aerosol algorithms in the M and A products counterbalance each other and lead to relatively small net differences between the two global products. These mechanisms are not fully understood at this time. Present analyses further support the point made elsewhere that for the overall quality of an aerosol product, especially one included in climate data records, sampling is at least as important as the degree of sophistication and complexity of the aerosol algorithm [*Ignatov et al., 2005*].

[73] Both anonymous reviewers of this paper wanted to see a more definitive statement on the relative contribution of sampling and aerosol algorithm to the observed cross-platform differences. This is a valid wish, but it cannot be easily addressed using the CERES SSF data where these two effects have been convolved. The most direct answer would involve application of the two aerosol algorithms to the same set of MODIS pixels, identified as cloud and glint-free by either the M\*D04 or CERES cloud masks. These analyses are beyond the scope of this study, which was

aimed at evaluation of the two aerosol products available on the CERES SSF data sets, and will be subject of future work.

[74] In either case, it is felt that the current priorities in the aerosol remote sensing should be revisited. In particular, the emphasis should be redirected from the ever increasing level of complexity of the aerosol inversion algorithm toward development of more scientifically sound sampling strategies. The lognormal nature of aerosol optical depth must be considered in pursuing the optimal space-time averaging procedures, validation, and statistical analyses. Cloud screening schemes alternate to the current threshold-based techniques should be explored. In particular, aerosol retrievals in imager pixels contaminated with subpixel cloud should be explored, in addition to the cloud retrievals in such pixels [*Coakley et al., 2005*]. These efforts would eventually lead to in-depth understanding and unification of the sampling procedures, and more continuous treatment of the “cloud-aerosol” gray zone.

[75] Satellite aerosol products are complex combinations of input data, sampling, and aerosol algorithms. These three factors are not fully independent and may interfere in a complicated way. A comprehensive system of quality control/assurance of each global product is thus needed that includes a set of self- and cross-consistency checks that are global in their nature. Examples of such checks are presented in this paper. These checks are not intended to replace the customary validation against ground-based Sun photometers which is considered the ultimate test for satellite retrievals. Rather, the two techniques should be used in concert with each other. In comparing different data sets using their intersection subsamples (cross-platform or cross-product comparisons, or validation against ground truth data), one must ensure that the intersection sample is statistically representative of the full data set being compared or validated.

[76] **Acknowledgments.** This work was funded by the NASA Science Mission under the CERES Project including NASA contract L-90987C. The Terra and Aqua CERES SSF data used in this study were obtained from the Atmospheric Sciences Data Center at NASA Langley Research Center. We thank N. Loeb for his critical support of the proposal to keep two aerosol products on the Terra and Aqua CERES SSF data sets and for helpful discussions; D. Tanré, Y. Kaufman and I. Laszlo for advice; and E. Geier and K. Morris for the help with CERES SSF data access. Thanks go to two anonymous reviewers of this manuscript who made a number of excellent points and suggestions. We tried to answer their questions fully and hope that the text is more readable now. The views, opinions, and findings contained in this report are those of the authors and should not be construed as an official NOAA or U.S. Government position, policy, or decision.

## References

- Ackerman, S. A., K. I. Strabala, W. P. Menzel, R. A. Frey, C. C. Moeller, and L. E. Gumley (1998), Discriminating clear-sky from clouds with MODIS, *J. Geophys. Res.*, *103*(D24), 32,139–32,158.
- Brennan, J., Y. Kaufman, I. Koren, and R. Li (2005), Aerosol-cloud interaction—Misclassification of MODIS clouds in heavy aerosol, *IEEE Trans. Geosci. Remote Sens.*, *43*(4), 1–5, doi:10.1109/TGRS.2005.844662.
- Brindley, H., and A. Ignatov (2006), Retrieval of mineral aerosol optical depth and size information from Meteosat second generation SEVIRI data, *Remote Sens. Environ.*, *102*, 344–363.
- Coakley, J., M. Friedman, and W. Tahnk (2005), Retrieval of cloud properties for partly cloudy imager pixels, *J. Technol.*, *22*(1), 3–17, doi:10.1175/JTECH-1681.1.
- Geier, E. B., R. N. Green, D. P. Kratz, P. Minnis, W. F. Miller, S. K. Nolan, and C. B. Franklin (2003), CERES data management system: Single Satellite Footprint TOA/surface fluxes and clouds (SSF) collection docu-

- ment, release 2, version 1, 212 pp. and appendixes, NASA Langley Res. Cent., Hampton, Va. (Available at [http://asd-www.larc.nasa.gov/ceres/collect\\_guide/SSF\\_CG.pdf](http://asd-www.larc.nasa.gov/ceres/collect_guide/SSF_CG.pdf))
- Ichoku, C., L. A. Remer, and T. F. Eck (2005), Quantitative evaluation and intercomparison of morning and afternoon Moderate Resolution Imaging Spectroradiometer (MODIS) aerosol measurements from Terra and Aqua, *J. Geophys. Res.*, *110*, D10S03, doi:10.1029/2004JD004987.
- Ignatov, A. (2002), Sensitivity and information content of aerosol retrievals from AVHRR: Radiometric factors, *Appl. Opt.*, *41*(6), 991–1011.
- Ignatov, A., and L. Stowe (2002a), Aerosol retrievals from individual AVHRR channels. Part I: Retrievals algorithm and transition from Dave to 6S radiative transfer model, *J. Atmos. Sci.*, *59*(3), 313–334.
- Ignatov, A., and L. Stowe (2002b), Aerosol retrievals from individual AVHRR channels. Part II: Quality control, probability distribution functions and consistency checks of retrievals, *J. Atmos. Sci.*, *59*(3), 335–362.
- Ignatov, A., L. Stowe, S. Sakerin, and G. Korotaev (1995), Validation of the NOAA/NESDIS satellite aerosol product over the North Atlantic in 1989, *J. Geophys. Res.*, *100*(D3), 5123–5132.
- Ignatov, A., I. Laszlo, E. Harrod, K. Kidwell, and G. Goodrum (2004a), Equator crossing times for NOAA, ERS, and EOS Sun-synchronous satellites, *Int. J. Remote Sens.*, *25*(23), 5255–5266.
- Ignatov, A., J. Sapper, I. Laszlo, N. Nalli, and K. Kidwell (2004b), Operational Aerosol Observations (AEROBS) from AVHRR/3 onboard NOAA-KLM satellites, *J. Technol.*, *21*(1), 3–26.
- Ignatov, A., P. Minnis, N. Loeb, B. Wielicki, W. Miller, S. Sun-Mack, D. Tanré, L. Remer, I. Laszlo, and E. Geier (2005), Two MODIS aerosol products over ocean on the Terra and Aqua CERES SSF datasets, *J. Atmos. Sci.*, *62*(4), 1008–1031, doi:10.1175/JAS3383.1.
- Kaufman, Y. J., B. N. Holben, D. Tanré, I. Slutsker, A. Smirnov, and T. F. Eck (2000), Will aerosol measurements from Terra and Aqua polar orbiting satellites represent the daily aerosol abundance and properties?, *Geophys. Res. Lett.*, *27*(23), 3861–3864.
- Li, R.-R., Y. J. Kaufman, B. C. Gao, and C. O. Davis (2003), Remote sensing of suspended sediments and shallow coastal waters, *IEEE Trans. Geosci. Remote Sens.*, *41*(3), 559–566, doi:10.1109/TGRS.2003.810227.
- Martins, J., D. Tanré, L. Remer, Y. Kaufman, S. Mattoo, and R. Levy (2002), MODIS cloud screening for remote sensing of aerosols over oceans using spatial variability, *Geophys. Res. Lett.*, *29*(12), 8009, doi:10.1029/2001GL013252.
- Matthias, V., and J. Bösenberg (2002), Aerosol climatology for the planetary boundary layer derived from regular lidar measurements, *Atmos. Res.*, *63*(3–4), 221–245.
- Minnis, P., D. F. Young, S. Sun-Mack, Q. Z. Trepte, Y. Chen, R. R. Brown, S. Gibson, and P. Heck (2004), Diurnal, seasonal, and interannual variations of cloud properties derived for CERES from Imager data, paper presented at 13th AMS Conference on Satellite Meteorology and Oceanography, *Am. Meteorol. Soc.*, Norfolk, Va, 20–24 Sept.
- Myhre, G., et al. (2004), Intercomparison of satellite retrieved aerosol optical depth over the ocean, *J. Atmos. Sci.*, *61*, 499–513.
- O'Neill, N., A. Ignatov, B. Holben, and T. Eck (2000), The log-normal distribution as a reference for reporting aerosol optical depth statistics: Empirical tests using multi-year, multi-site AERONET Sun photometer data, *Geophys. Res. Lett.*, *27*(20), 3333–3336.
- Remer, L. A., et al. (2002), Validation of MODIS aerosol retrievals over ocean, *Geophys. Res. Lett.*, *29*(12), 8008, doi:10.1029/2001GL013204.
- Remer, L. A., et al. (2005), The MODIS aerosol algorithm, products, and validation, *J. Atmos. Sci.*, *62*(4), 947–973, doi:10.1175/JAS3385.1.
- Szewczyk, Z., G. L. Smith, and K. J. Priestley (2005), Validation of Clouds and Earth Radiant Energy System instruments aboard the Terra and Aqua satellites, *J. Geophys. Res.*, *110*, D02103, doi:10.1029/2004JD004776.
- Tanré, D., Y. J. Kaufman, M. Herman, and S. Mattoo (1997), Remote sensing of aerosol properties over oceans using the MODIS/EOS spectral radiances, *J. Geophys. Res.*, *102*(D14), 16,971–16,988.
- Wielicki, B. A., B. R. Barkstrom, E. F. Harrison, R. B. Lee III, G. L. Smith, and J. E. Cooper (1996), Clouds and the Earth's Radiant Energy System (CERES): An Earth Observing System experiment, *Bull. Am. Meteorol. Soc.*, *77*(11), 853–868.

---

A. Ignatov, Office of Research and Applications, NESDIS, NOAA, E/RA3, Room 603, WWB, 5200 Auth Road, Camp Springs, MD 20746-4304, USA. (alex.ignatov@noaa.gov)

W. F. Miller, P. Minnis, and B. A. Wielicki, Atmospheric Sciences, NASA LARC, Hampton, VA 23681, USA.

L. Remer, NASA GSFC, Code 913, Building 33, Room C323, Greenbelt, MD 20771, USA.